NAR Cancer, 2024, **6**, zcae044
https://doi.org/10.1093/narcan/zcae044
Advance access publication date: 28 November 2024
DNA Damage Sensing and Repair

OXFORD

RAD51 recruitment but not replication fork stability associates with PARP inhibitor response in ovarian cancer patient-derived xenograft models

Francien Talens[1], Vivian Oliviera Nunes Teixeira[1], Yannick P. Kok[1], Mengting Chen[1], Efraim H. Rosenberg[2], Rashmie Debipersad[2], Evelien W. Duiker[3], Nathalie van den Tempel[1], Marketa Janatova[4], Petra Zemankova[4,5], Petra M. Nederlof[2], G. Bea A. Wisman[6], Zdenek Kleibl[4,5], Steven de Jong[1] and Marcel A.T.M. van Vugt[1,*]

[1]Department of Medical Oncology, University Medical Center Groningen, University of Groningen, Hanzeplein 1, 9713GZ Groningen, the Netherlands
[2]Department of Pathology, Netherlands Cancer Institute, Plesmanlaan 121, 1066CX Amsterdam, the Netherlands
[3]Department of Pathology and Medical Biology, University Medical Center Groningen, University of Groningen, Hanzeplein 1, 9713GZ Groningen, the Netherlands
[4]Institute of Medical Biochemistry and Laboratory Diagnostics, First Faculty of Medicine, Charles University and General University Hospital in Prague, Katerinska 32, 128 00 Prague, Czech Republic
[5]Department of Pathophysiology, First Faculty of Medicine, Charles University, U Nemocnice 5, 128 00 Prague, Czech Republic
[6]Department of Gynecology and Obstetrics, University Medical Center Groningen, University of Groningen, Hanzeplein 1, 9713GZ Groningen, the Netherlands

[*]To whom correspondence should be addressed. Tel: +31 50 3615002; Email: m.vugt@umcg.nl

Abstract

Poly(ADP-ribose) polymerase (PARP) inhibitors (PARPis) are currently used to treat *BRCA1/2* mutant cancers. Although PARPi sensitivity has been attributed to homologous recombination (HR) defects, other roles of HR factors have also been linked to response to PARPi, including replication fork protection. In this study, we investigated PARPi sensitivity in ovarian cancer patient-derived xenograft (PDX) models in relation to HR proficiency and replication fork protection. Analysis of *BRCA1/2* status showed that in our cohort of 31 ovarian cancer PDX models 22.6% harbored a *BRCA1/2* alteration (7/31), and 48.3% (15/31) were genomically unstable as measured by copy number alteration analysis. *In vivo*, PARPi olaparib response was measured in 15 selected PDX models. Functional assessment of HR using *ex vivo* irradiation-induced RAD51 foci formation identified all olaparib-sensitive PDX models, including four models without *BRCA1/2* alterations. In contrast, replication fork protection or replication speed in *ex vivo* tumor tissue did not correlate with olaparib response. Targeted panel sequencing in olaparib-sensitive models lacking *BRCA1/2* alterations revealed a MUS81 variant as a possible mechanism underlying PARPi sensitivity. Combined, we show that *ex vivo* RAD51 analysis effectively predicts *in vivo* olaparib response and revealed a subset of PARPi-sensitive, HR-deficient ovarian cancer PDX models, lacking a BRCA1/2 alteration.

Graphical abstract

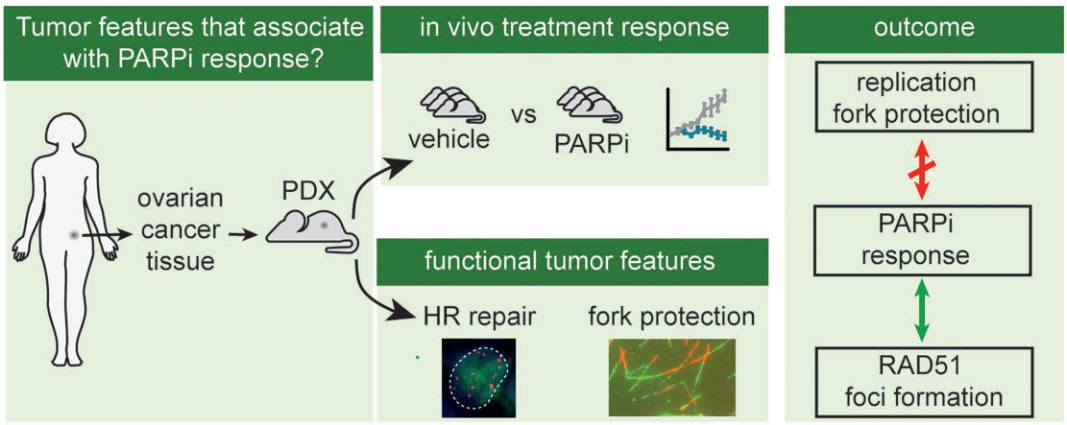

Received: May 21, 2024. **Revised:** October 23, 2024. **Editorial Decision:** October 25, 2024. **Accepted:** October 28, 2024

Introduction

Ovarian cancer is the eighth most common cancer type among women worldwide and survival rates have hardly improved over the last decades (1). High-grade serous ovarian cancer (HGSOC) is the most common subtype of ovarian cancer (∼70%) and is frequently diagnosed in an advanced stage, with the majority of patients being diagnosed with stage >IIB disease. Importantly, patients with metastatic HGSOC have a 5-year relative survival rate of ∼30%. Current treatment of HGSOC combines surgery with (neo)adjuvant platinum-based chemotherapy. Approximately 15–20% of HGSOC are characterized by *BRCA1/2* mutations or *BRCA1* promoter hypermethylation (2). In line with this notion, females carrying a germline *BRCA1* or *BRCA2* mutation have a highly increased lifetime risk to develop breast and/or ovarian cancer (3,4).

BRCA1 and BRCA2 function in homologous recombination (HR), an error-free pathway to repair toxic DNA double-stranded breaks (DSBs) (5). HR proteins, such as BRCA1 and BRCA2, have additional functions in preventing chromosomal instability, including preventing the degradation of nascent DNA at stalled replication forks (6,7) and suppressing the formation of single-stranded (ss)DNA gaps in the lagging strand during DNA replication (8–10). Tumor cells with mutations in these HR factors are sensitive to treatment with inhibitors of the Poly(ADP-ribose) polymerase (PARP) enzyme, which functions in single-strand break (SSB) repair (11,12). Several PARP inhibitors (PARPis), including olaparib, niraparib and rucaparib, have been clinically evaluated and treatment with these drugs improved progression-free survival in patients with *BRCA1/2* mutated ovarian cancer and therefore resulted in FDA approval. Currently, the PARPi olaparib is approved for use in *BRA1/2* mutant ovarian and *BRCA1/2* mutant HER2-negative metastatic breast cancers (13), whereas niraparib is approved for all ovarian cancers that responded to platinum-based therapy. Additionally, olaparib and rucaparib are indicated for castration-resistant *BRCA1/2* mutant prostate cancer.

How exactly PARPis exert their cytotoxic effects is a topic of ongoing debate. Initial hypotheses involved the accumulation of ssDNA breaks, which lead to DSBs at sites of ongoing replication (11,12,14). As a logical consequence in this model, the formation of DSBs would necessitate BRCA1/2 and related factors for accurate repair through HR. Subsequently, PARPis were found to trap PARP molecules onto DNA and perturb DNA replication (15), and that BRCA1/2 prevent the nucleolytic degradation of stalled replication forks (7). Combined, these findings gave rise to a model in which PARP inhibition leads to stalled replication forks that require functional BRCA1/2 for protection and that the sensitivity to PARPis is determined by the ability of cells to protect stalled replication forks (16,17). A more recent study revealed that PARP1 slows down replication speed (18), and that accelerated replication velocity induced by PARP inhibition leads to DNA lesions. Along this line, BRCA1/2 was shown to prevent PARPi-induced ssDNA gaps during replication (19). Moreover, levels of ssDNA gaps, rather than DSB accumulation, were shown to associate with PARPi response (20). Finally, PARP1 was demonstrated to protect the replisome from transcription-replication conflicts, and conversely, PARP inhibition induces replication-transcription conflicts that underlie cytotoxicity in HR-deficient cancer cells (21).

Also several mechanisms have been described by which HR-defective tumors become resistant to PARPi treatment. Reversion mutations in *BRCA1/2* form a main mechanism of acquired resistance in the clinic (22). Also, mutations in other genes have been shown to confer resistance to PARP inhibition. For instance, inactivation of *TP53BP1* (23,24), *REV7* (25) or Shieldin complex genes (26,27) can restore HR in *BRCA1* mutant cancer cells and leads to PARPi resistance in experimental models. Similarly, mutations in the CST genes rescue HR in *BRCA1* mutant cancer cells and lead to PARPi insensitivity (28). Because inactivation of the above-mentioned genes partially restores HR, these findings pointed at defective HR as a determinant of PARPi sensitivity. However, loss of 53BP1 also rescues Okazaki fragment processing and ssDNA gap formation, providing an alternative explanation for the observed PARPi resistance (19). In addition, mutations in *PAXIP2* were described to rescue replication fork stability in *BRCA2* mutant cells and thereby determine PARPi sensitivity (16). These latter observations suggest that mechanisms beyond HR determine PARPi sensitivity. Of note, a separation-of-function mutant of *Brca2* that is HR proficient but cannot suppress ssDNA gaps or mediate fork protection does not confer PARPi sensitivity *in vivo*, while a *Brca2* mutant that is defective in HR does lead to PARPi sensitivity (29), again pointing at HR as the main determinant of PARPi sensitivity.

A solid understanding of the mechanisms that drive PARPi sensitivity and resistance is needed to effectively identify PARPi eligible patients. Currently used homologous recombination deficiency (HRD) tests to select patients for PARPi treatment are based on *BRCA1/2* status or genomic scars (30). For example, the myChoice HRD test combines *BRCA1/2* mutation status with different measurements of genomic instability in tumor cells, including loss-of-heterozygosity (LOH), telomeric imbalance and large-scale state transitions, and has demonstrated varying results in predicting platinum response in triple-negative breast cancer (TNBC) (31,32). Intriguingly, this test did not predict response to the PARPi niraparib in platinum-sensitive ovarian cancer (33).

In a different approach, algorithms were developed on whole-genome sequencing profiles to distinguish *BRCA1/2*-mutated breast cancers from sporadic breast cancer (34,35). Of these, the HRDetect algorithm was able to detect HR-deficient tumors without *BRCA1/2* mutations in different cancer types and HRDetect scores were associated with response to platinum-based chemotherapy in advanced breast cancer, independently of *BRCA1/2* mutation status (36). These approaches are highly relevant, because PARPi treatment is expected to also be effective in tumors that lack a *BRCA1/2* mutation but with mutation or epigenetic silencing of other HR genes, including *PALB2*, *CHEK1/2*, *RAD51C*, *RAD51D* and *ATM* (2,37–40). In line with this notion, several clinical trials have shown proven efficacy of PARPi beyond *BRCA1/2*-mutated ovarian cancer (33,41). Based on these findings, all patients with HRD tumors, also those caused by mutations other than *BRCA1/2* alterations, are currently eligible for PARPi treatment. Yet, proper selection methods are needed to select those patients with high likelihood for treatment benefit.

Since *BRCA1/2* mutation analysis nor analysis of genomic features associated with HRD per se reflects actual HR functionality, these assays may not be effective in proper selection

of patients that benefit from PARPi treatment. Therefore, an *ex vivo* functional test for HR pathway proficiency was developed, the RECAP assay, which assesses foci formation of the RAD51 recombinase (42). The loading of RAD51 onto ssDNA at DSBs is a crucial step in HR and can be visualized with immunofluorescence (43). Although this approach does not take into account all functions of HR proteins, including replication fork protection or ssDNA suppression, this assay successfully identified HRD breast cancers that lacked a *BRCA1/2* mutation but were not able to recruit RAD51 foci and were therefore considered HRD (44,45). Furthermore, formation of RAD51 foci correlated to PARPi resistance in *BRCA1/2* mutant breast cancer models, regardless of the underlying resistance mechanism (46,47). Also, functional HR testing could predict platinum sensitivity in ovarian cancer patients (48). In primary cultures derived from ascitic fluid from ovarian cancer patients, RAD51 foci formation correlated to *in vitro* PARPi response (49). However, it remains unclear whether *in vivo* responses to PARPi can be predicted using functional HR assays in ovarian cancer models. Morerover, other functions of BRCA1/2 such as replication fork protection have to date not been included in functional assays to predict PARPi response in clinically relevant cancer models.

In this study, we performed a functional assessment of HR using the RAD51-based RECAP assay along with functional analysis of replication fork protection in a cohort of patient-derived xenograft (PDX) models of ovarian cancer. These parameters were correlated to *in vivo* olaparib sensitivity in PDX models of ovarian cancer. We show that the RECAP assay is superior in identifying olaparib-sensitive PDX models, when compared to *BRCA1/2* status, copy number alteration (CNA) profiles and replication fork stability. These results demonstrate that clinical evaluation of functional HR assessment is warranted to select patients with ovarian cancer for PARPi treatment.

Materials and methods

Patient-derived tumor xenograft (PDX) mouse models

Cryopreserved tumor pieces from a cohort of ovarian cancer patients were thawed for implantation into 6- to 10-week-old female NOD.Cg-Prkdcscid Il2rgtm1Wjl/SzJ (NSG) mice (internal breed, Central Animal Facility, University Medical Center Groningen), as described previously (50). Typically, one tumor piece was subcutaneously implanted on one side of the flank and surgery was performed as previously described (50). Mice received sterilized food and water ad libitum and were kept under pathogen-free conditions in the Central Animal Facility at the University Medical Center Groningen. Animal experiments were approved by the Institutional Animal Care and Use Committee of the University of Groningen and followed the EU Guideline on Animal Experiments. Mouse experiments were divided into two phases: an expansion phase and a treatment phase. For the expansion phase, two mice were implanted with F1 or F2 ovarian cancer specimens. When tumors reached a volume of ∼1000 mm^3, mice were terminated and tumors were used for implantation into 14 recipient mice for the treatment phase. In parallel to implantation for treatment studies, tumor pieces were used for *ex vivo* DNA fiber assay analysis and the RECAP assay.

Analysis of copy number alterations (CNAs) and genomic status of BRCA1/2

For analysis of CNAs and *BRCA1/2* status, frozen tissue slices (10 μm) were cut from F1 tumor material that was stored at −80°C. Tissue slices were stained for hematoxylin and eosin (H&E), and were analyzed by a gynecologic pathologist to determine tumor cell percentage. Genomic DNA was isolated using the QIAamp DNA mini kit (Qiagen) according to manufacturer's protocol. For *BRCA1/2* mutational analysis, samples were sequenced using Multiplicom BRCA MASTR for NGS. To determine *BRCA1* promoter methylation, MS-MLPA (SALSA MLPA Probemix ME001, MRC Holland) was performed as described. Cartagenia Bench was used for variant calling and results were compared with the Dutch national *BRCA1/2* database, incorporated in the Leiden Open Variation Database LOVD v.3.0 (51).

Low-coverage whole-genome sequencing and *BRCA1/2*-like classification was performed as described previously (52). Samples were classified as *BRCA*-like if the predicted probability was >0.5 and non–*BRCA*-like if the predicted probability was ≤ 0.5. BRCA1 and BRCA2 scores are listed in Supplementary Table S1. Based on CNAs profiles, models were classified by visual interpretation into five categories (A–E), ranging from 'flatliner' profiles containing no CNAs (category A), few aberrations (categories B and C) and profiles with many aberrations and intrachromosomal rearrangements (categories D and E). Examples of CNA profiles can be found in Supplementary Figure S1.

MSI analysis

Microsatellite instability (MSI) was assessed by testing tumor DNA in a pentaplex polymerase chain reaction (PCR)-based assay using fluorescent labelled primers of five mononucleotide repeat targets (BAT25, BAT26, NR24, NR21, NR27), followed by fragment analysis. In case of instability in two markers or more, the tumor is defined as MSI-high. Instability of only one marker is considered MSI-low. When five markers are without instability the tumor is defined as MS stable (MSS).

In vivo evaluation of PARPi response

Mice were closely observed, weighted and tumor size was measured at least once a week. Tumor size was measured using a caliper, and volume was calculated using the following formula: $(width^2 \times length)/2$. When tumors reached a volume of ∼200 mm^3, mice were distributed into a vehicle treatment group (10% dimethyl sulfoxide [DMSO], 10% 2-hydroxypropyl-β-cyclodextrin (HPBCD) in phosphate saline buffer [PBS]) or olaparib treatment group (100 mg/kg diluted in 10% DMSO, 10% HPBCD in PBS). Treatments were administered through intraperitoneal injection, comparable to other olaparib *in vivo* PDX studies (53). Mice were divided into treatment groups based on tumor size to maintain a comparable mean tumor size in both groups at start of treatment. Treatment was administered using intraperitoneal injections for six times a week. After 28 days, mice were terminated by cervical dislocation under isoflurane anesthesia. Tumors were harvested, weighted and cut into two pieces: one piece was snap frozen and kept in −80°C whereas the other piece

was stored in formalin. Following the guidelines of animal experimentation, the following humane endpoints were followed to avoid unnecessary suffering of animals: tumor size > 1500 cm^3, weight loss > 15%, ulceration of tumors, observation of hunched posture or altered behavior. Tumor growth (%) during treatment was calculated by comparing the tumor volume at the end of treatment to tumor volume at day 0. The response to olaparib for each PDX model was calculated by comparing the mean tumor growth in the olaparib-treated group with the mean tumor growth in the DMSO-treated group as a percentage. Adapted Response Evaluation Criteria in Solid Tumors (RECIST) guidelines were used to classify PDX models as responders to olaparib (54). A model was considered sensitive when a decrease of at least 30% (partial response, RECIST) in mean tumor growth upon olaparib treatment was observed compared to DMSO treatment.

Functional RAD51 (RECAP) assay

The RECAP (REpair CAPacity) assay, a functional assay to assess RAD51 foci formation in tumor tissue after *ex vivo* irradiation, was performed as described previously (42). Fresh PDX tumor tissue harvested from mice was cut into 2–3 mm pieces and placed in 6-well plates with Roswell Park Memorial Institute (RPMI) medium, supplemented with 10% fetal calf serum (FCS) and 1% penicillin/streptomycin (P/S) within 4 h after resection. After irradiation using a $Cesium^{137}$ source (5 Gy, IBL 637 $Cesium^{137}$ gamma-ray machine), tumor pieces were incubated for 3 h at 37°C. Tumor pieces were then put in formalin overnight and imbedded in paraffin. Tissue sections were deparaffinized with xylene and hydrated with decreasing concentrations of ethanol. For antigen retrieval, sections were microwaved for 12 min at 100°C in retrieval solution (DAKO, #S2367). Sections were cooled down for 20 min, permeabilized with 0.2% Triton-X-100 in PBS for 20 min at room temperature, washed once with PBS and incubated with DNAse I (1000 U/ml, Roche, #04 536 282 001) for 1 h at 37°C in an incubator. Slides were incubated in blocking buffer (1% BSA, 2% FCS in PBS) for at least 30 min. Primary antibodies were diluted in blocking buffer and incubated at room temperature for 1 h. Primary antibodies used were mouse anti-human RAD51 (1:200; Genetex, #gtx70230 clone 14B4) and rabbit anti-human Geminin (1:400, Protein Tech, #10 802). Secondary antibodies AlexaFluor 594-conjugated goat anti-mouse (1:1000, Invitrogen, #A11005) and AlexaFluor 488-conjugated goat anti-rabbit (1:1000, Invitrogen, #A11034) were diluted in blocking buffer and incubated for 1 h at room temperature. Sections were air dried in the dark for 30 min and mounted with ProLong Diamond Antifade Mountant reagent with DAPI (4′,6-diamidino-2-phenylindole, Invitrogen, #P36966) and stored overnight at 4°C. RAD51 staining was quantified by scoring the percentage of geminin-positive cells with ≥5 foci/cell. Tumors with <20% of geminin-positive cells with ≥5 RAD51 foci/cell were classified as HRD, as has been used in other studies (42,44,55). At least 30 geminin-positive cells were analyzed on at least two different slides. Immunofluorescence images were acquired on a Leica DM-6000RXA microscope using LAS X software.

DNA fiber assay

Fresh tumor material harvested from mice was cut into pieces of ∼2–3 mm each, while kept in RPMI medium supplemental with 10% FCS and 1% P/S. Tumors were dissociated into single-cell suspensions using the Human Tumor Dissociation Kit, according to manufacturer's instructions (Macs Miltenyi Biotec, #130–095-929). Human cells were enriched from the cell pool using the Mouse Cell Depletion Kit (Macs Miltenyi Biotec, # 130–104-694). After isolation, tumor cells were incubated in 6-well plates and resuspended in RPMI medium supplemented with 10% FCS and 1% P/S, containing CldU (25 μM) for 30 min at 37°C. After extensive washing with medium, cells were incubated in medium supplemented with IdU (250 μM) for 45 min at 37°C. If indicated, IdU was then washed out, and left untreated or treated with hydroxyurea (HU, 5 mM) for 3 h at 37°C. Cells were subsequently lysed on glass slides in lysis buffer (200 mM Tris–HCl, pH 7.4, 50 mM EDTA, 0.5% SDS) and DNA fibers were spread by tilting the glass slides ∼15 degrees. At least three slides of each condition were made. Fibers were fixed with methanol/acetic acid (3:1) for 10 min and then stored at 4°C. Prior to immunolabeling, slides were washed with water and incubated with 2.5 M HCl for 75 min to denature the DNA. Slides were then washed with PBS and incubated with blocking solution (1% bovine serum albumin [BSA], 0.1% Tween-20 in PBS) for 30 min. Next, slides were incubated with primary antibodies rat-anti-BrdU (1:1000, Abcam #ab6326) and mouse-anti-BrdU (1:250, BD Biosciences #347 580) for 1 h, followed by incubation with secondary antibodies AlexaFluor 488-conjugated goat anti-rat (1:500, Invitrogen #A11006) and AlexaFluor 594-conjugated goat anti-mouse (1:500, Invitrogen #A11005) for 90 min. Immunofluorescence images were acquired on a Leica CTR6000 microscope using LAS X software (Leica Application Suite X). Fiber length was measured using ImageJ software. A conversion factor of 1 μm = 2 kb was used, as described previously (56).

EdU/cytokeratin immunofluorescence staining

Single-dissociated cells used for DNA fiber analyses were incubated with EdU for 1 h at 37°C. Cells were harvested and cytospinned on glass slides. Cells were fixed with 3.7% formaldehyde in PBS for 15 min at room temperature. Until staining, slides were stored in −80°C. For EdU staining, cells were permeabilized with 0.5% Triton-X-100 in PBS for 20 min. Subsequently, cells were incubated with a reaction cocktail for 30 min in the dark consisting of 116.3 mM Tris–HCl pH 8.5, 100 mM $CuSO_4$, Alexa fluor azide (0.24 μl per reaction) and 100 mM ascorbic acid in H_2O. Washing steps were performed with 3% BSA in PBS. For further staining, cells were washed with PBS and permeabilized with 0.1% Triton-X-100 in PBS for 5 min. Blocking was performed in 2.5% BSA–0.05% Tween-20 in PBS for 1 h. Slides were incubated with primary antibody anti-pan cytokeratin (1:50, AE1AE3, DAKO) in 0.05% Tween-20 in PBS overnight at 4°C followed by secondary Alexa-conjugated antibodies for 1 h at room temperature. Immunofluorescence images were acquired on a Leica CTR6000 microscope using LAS X software (Leica Application Suite X).

Targeted DNA sequencing

Multi-gene panel sequencing of DNA from F1 PDX tumor material was performed using the CZECANCA panel (57). The procedure was performed as described previously with the following minor modifications. The CZECANCA panel version 1.2 was used, which targets 226 genes instead of

219 genes. The list of targeted genes included in CZECANCA panel version 1.2 can be found in Supplementary Table S2. Sequencing was performed on the Illumina NextSeq platform. Coverages exceeded 500× for the majority of targeted sequences. In total, 39 341 variants were called and the following filters were applied: sequencing errors/low quality variants (quality < 150 from GATK software pipeline), frequent variants (mutation allele frequency, MAF > 0.05 in 1000 Genomes project and ESP6500), variants with difficult interpretation (extragenic, intronic [except splicing alterations], UTR), variants described in ClinVar as benign or likely benign, or presented in non-cancer and general population controls. Remaining 22 variants were validated using the Integrative genomics viewer (IGV) and are listed in Table 2.

MUS81 knockout generation in U2OS

The human osteosarcoma cell line U2OS was obtained from ATCC (#HTB-96) and was cultured in Dulbecco's Minimum Essential Medium (DMEM, Thermofisher), supplemented with 10% FCS, 1% penicillin and 1% streptomycin (Gibco). A single-guide RNA (sgRNA) targeting MUS81 (GTTTAGGGAAGTGACCCAGG) was cloned into lenti-CRISPRv2 puro (Addgene #98 290). U2OS cells were transiently transfected with sgMUS81 using Fugene (Promega), according to manufacturer's protocol. Two days later, cells were selected by puromycin (1 μg/ml, Sigma) for 4 days and plated in 96-well plates to generate single clones.

MUS81 variant analysis

eHAP1 parental and *MUS81*^{KO} cells were a kind gift from Dr S. West and K. Fugger (Crick Institute, London, UK) (58), and were cultured in Iscove Modified Dulbecco Media (IMDM, Thermofisher), supplemented with 10% FCS, 1% penicillin and 1% streptomycin (Gibco). pLNCX2-GFP-MUS81-wt was synthesized by Eurofins Genomics (Germany). eHAP1 cells were transduced with pLNCX2-GFP-MUS81-wt or pLNCX2-GFP-MUS81-R496Q. The R496Q mutation was introduced in pLNCX2-GFP-MUS81-wt by mutagenesis PCR, using the following primers: forward: ′TGGGGAGAAGGCAGCAGCCCTG GTGGATCAATACAGCACCC′ reverse ′GGGTGCTGTATT GATCCACCAGGGCTGCTGCCTTCTCCCCA′. HEK293T cells were transfected with pLNCX2-GFP-MUS81-wt or R496Q along with lentiviral packing plasmids as described previously. Virus was harvested at 48 h after transfection for transduction. eHAP1-*MUS81*^{KO} cells were transduced for 24 h. At 48 h after transduction of eHAP1-*MUS81*^{KO}, GFP-positive cells were sorted using a Sony SH800 flow cytometry cell sorter.

MTT assays

U2OS WT and *MUS81* knockout cells were plated in 96-well at 500 cells per well and allowed to attach for 24 h. Olaparib or cisplatin was added to U2OS cells at indicated concentrations for 3 days. eHAP1 cells were plated in 96-well at 500 cells per well and allowed to attach for 24 h. Olaparib was added to eHAP1 cells at indicated concentrations for 4 days. Next, cells were incubated with methylthiazol tetrazolium (MTT, final concentration 0.5 mg/ml) for 3 h. After removal of medium, formazan crystals were dissolved in DMSO. Absorbance was measured at 520 nm, and was quantified with a Benchmark III spectrophotometer (Bio-Rad). Results represent $n = 3$ independent replicates for U2OS cells and $n = 5$ independent replicates for eHAP1 cells. Background-ground corrected MTT conversion data were normalized to DMSO treated conditions of wt-eHAP1 cells or wt-U2OS cells. For analysis of area under the curve (AUC), default setting of AUC analysis in Graphpad Prism (version 8.4.2) were used on non-fitted curves and equally spaced *X*-axis values.

RAD51 staining

U2OS WT and *MUS81* knockout cells were seeded on glass coverslips. On the next day, cells were irradiated (5 Gy) using a CIS international/IBL 637 cesium^{137} source. At 3 h after irradiation, cells were fixed with 2% paraformaldehyde, permeabilized in 0.1% Triton X-100 in PBS, blocked in 4% BSA in PBS and incubated with primary antibodies against RAD51 (GeneTex, #gtx70230, 1:200) and Geminin (Proteintech, #10 802, 1:200) overnight. Secondary antibodies Alexa-488 (anti-mouse, 1:500) and Alexa-647 (anti-rabit, 1:500) were used and slides were stained with DAPI. Images were made using a Leica DM6000B microscope with a ∼63x immersion objective.

Statistical analysis

All statistical tests were performed using GraphPad Prism version 7.0. Parametric data were analyzed using unpaired t-tests (two-tailed), one-way ANOVA or two-way ANOVA. Non-parametric data were analyzed using Mann–Whitney tests. Data are presented as means with standard error of the mean (SEM) or median with percentiles for non-parametric data. Correlations were calculated using Spearman's test.

Results

Characterization and selection of ovarian cancer PDX models

To study the response of ovarian cancers towards the PARPi olaparib, we studied 31 pre-established ovarian PDX models (50). Based on retrieved pathology reports of the primary tumor, 21 out of 31 PDX models represented serous ovarian cancer, of which 20 were HGSOC. Approximately 10 out of 31 PDX models represented other ovarian cancer subtypes, including endometrioid adenocarcinoma ($n = 6$), carcinosarcomas ($n = 2$) or mucinous adenocarcinoma ($n = 1$) (Table 1). Out of 31 PDX models, 7 models harbored a pathogenic *BRCA1* or *BRCA2* alteration (Table 1). Of these models, PDX177 and PDX203 had a *BRCA2* deletion with a high allele frequency, well above 50% (Table 1). The other *BRCA1/2* alterations had allele frequency of ∼50%, and were considered heterozygous, without LOH. In addition to the observed genomic alterations, PDX84 showed *BRCA1* promoter hypermethylation, which is a commonly observed somatic mechanism of *BRCA1* gene silencing.

As a readout for genomic instability, CNA levels were determined through CNVseq (Supplementary Figure S1A). PDX models were classified in five categories ranging from 'flat-liner' profiles and profiles that contained very few CNAs (profile A) toward genomically unstable profiles with high amounts of CNAs (profile E). Classification was done without knowledge about other tumor characteristics, such as gene alterations and tumor type. In total, 15 models were considered genomically unstable, based on a CNA profile D or E. Notable, not all PDX models with *BRCA1/2*

Table 1. Tumor characteristics of PDX models included in the study. Highlighted models were included for *in vivo* PARPi sensitivity

PDX #	Tumor type	Grade	Stage	Tissue origin	Follow-up	*BRCA1/2 status*	CNV profile	MSI status	panel sequencing (sample #)	BRCA1/2 score (see also Supplementary Table S1)	Olaparib response	RAD51 assay (RECAP)
30	Serous cystadenocarcinoma	High	IIIC	Diagnostic laparotomy	Relapse after 24 months, deceased		D	MSS		B2-like		
37	Serous cystadenocarcinoma	High	IIIC	Diagnostic laparotomy	No signs of recurrence (2015)		E	MSS	S01	B2-like	sensitive	Defective
56	Serous cystadenocarcinoma	High	IIIC	Interval debulking	No signs of recurrence (2015)		D	MSS		B1-like	Insensitive	Proficient
60	Serous cystadenocarcinoma	High	IIA	Diagnostic laparotomy	Deceased, 17 months		C	MSS		B2-like		
61	Mucinous adenocarcinoma	Undifferentiated	IV	Diagnostic laparotomy	Deceased		C	MSS				
67	Serous cystadenocarcinoma	High	IIIC	Diagnostic laparotomy	No signs of recurrence (2015)		E	MSS	S02	B1 and B2-like	Sensitive	Defective
68	Ovarian carcinosarcoma	High	IIC	Diagnostic laparotomy	Recurrence 29 months after last chemo. Re-debulkin. Deceased 40 months		A	MSS			Insensitive	Proficient
70	Serous adenocarcinoma with partial oxyfile clearcell component	High	IIIA	Diagnostic laparotomy	Deceased		E	MSS		B2-like		
79	Serous cystadenocarcinoma	Low	IIIC	Diagnostic laparotomy	Bad response: Palliative situation		B	MSS				
81	Endometrioid adenocarcinoma	Moderate	IC	Diagnostic laparotomy	No signs of recurrence	BRCA1: Deletion c.1823delA: p.K608fs in exon 11 of 50%	A	MSI-H	S03		Insensitive	Proficient
84	Serous cystadenocarcinoma	High	IV	Diagnostic laparotomy	No signs of recurrence (2015)	BRCA1: promotor methylation	E	MSS		B1 and B2-like	Sensitive	Defective
102	Unknown			Diagnostic laparotomy	Unknown		A	MSS				
112	Endometrioid adenocarcinoma	High	IIIC	Diagnostic laparotomy	No signs of recurrence		A	MSS	S04		Insensitive	Proficient
130	Serous cystadenocarcinoma	High	IIIB	Diagnostic laparotomy	No signs of recurrence		C	MSS				
143	Serous cystadenocarcinoma	High	IIIC	Interval debulking	Deceased 11 months		E	MSS		B1-like	Insensitive	Proficient
157	Endometrioid adenocarcinoma	High	IV	Diagnostic laparotomy	Deceased 6 months		B	MSS		B1-like		
167	Endometrioid adenocarcinoma	Moderate	IA	Interval debulking	Recurrence 50 months		B	MSS				
171	Serous cystadenocarcinoma	High	III	Recurrence 2010	Recurrence 38 months, deceased 51 months		A	MSS				
174	Serous cystadenocarcinoma	High	IV	Interval debulking	Good response		D	MSS	S05	B2-like	Sensitive	Defective
176	Serous cystadenocarcinoma		IIIC	Diagnostic laparotomy	No signs of recurrence. Deceased 9 months		D	MSS	S06		Sensitive	Defective
177	Serous cystadenocarcinoma with partial clear cell differentiation	High	IIC	Diagnostic laparotomy	n.a.	BRCA2: Deletion c.1457delA: p.Q486fs in exon 10 of 97%	D	MSS	S07	B2-like	Sensitive	Defective

Table 1. Continued

PDX #	Tumor type	Grade	Stage	Tissue origin	Follow-up	*BRCA1/2 status*	CNV profile	MSI status	panel sequencing (sample #)	BRCA1/2 score (see also Supplementary Table S1)	Olaparib response	RAD51 assay (RECAP)
179	Serous cystadenocarcinoma	High	IIIC	Interval debulking	Interval: good clinical response, deceased 9 months		B	MSS				
187	Serous cystadenocarcinoma	High	IIIC	Interval debulking	Interval: good response		D	MSS			Insensitive	Proficient
188	Serous cystadenocarcinoma	High	IIIC	Primary debulking	Progression within 6 months after chemotherapy (deceased)		C	MSS		B2-like		
189	Endometrioid adenocarcinoma	High	IC	Diagnostic laparotomy	Disease free at last follow-up (10 months)	BRCA2: Deletion c.9097delA: p.T3033fs in exon 23 of 51%	B	MSI-H	S08			
191	Ovarian carcinosarcoma		IIIC	Primary debulking	Recurrence 20 months		D	MSS		B2-like	Insensitive	Proficient
193	Serous cystadenocarcinoma	High	IIIC	Diagnostic laparotomy	Adjuvant chemotherapy	BRCA1: Exon 3 duplication	E	MSS	S09	B1 and B2-like	Sensitive	Defective
195	Serous cystadenocarcinoma	High	IV	Diagnostic laparotomy	Complete debulking, adjuvant chemotherapy	BRCA1: Deletion c.5542del: p.Q1848fs in exon 24 of 51%	D	MSS	S10	B1 en B2-like	Sensitive	Defective
203	Serous cystadenocarcinoma	High	IIIC	Primary debulking	Disease-free at last follow-up (25 months)	BRCA2: Deletion c.7007_7007 + 1delinsTT, a splice mutation in exon 13 of 75%	D	MSS		B1 en B2-like		
207	Serous cystadenocarcinoma	High	IIIC	Diagnostic laparotomy	Disease-free at last follow-up (36 months)		A	MSS				
208	Endometrioid adenocarcinoma	Low	IIB	Diagnostic laparotomy	Disease-free at last follow-up (18 months)		A	MSS				

Abbreviations: MSI, microsatellite instable; MSS, microsatellite stable.
Color scheme:
Gray boxes: selected for *in vivo* analysis for olaparib sensitivity

alterations showed high levels of CNAs (i.e. PDX81, PDX189), in line with these models not representing HG-SOC but endometrioid tumors, and not having homozygous *BRCA1/2* alterations, likely caused by high microsatellite instability (MSI-high) (Table 1).

As BRCAness correlates with high levels of genomic instability and is associated with PARPi response, all tumor models with D or E CNA profiles were selected for *in vivo* assessment of olaparib sensitivity (34). Additionally, two ovarian cancer PDX models without *BRCA1/2* alterations and genomically stable profile (PDX68 and PDX112) were included for reference (Supplementary Figure S1B). Furthermore, all models that harbored a *BRCA1/2* alteration were included, regardless of their CNAs profile. Approximately 4 out of 19 PDX models that were selected for *in vivo* PARPi response assessment could not be analyzed, either due to limited tissue availability (PDX203), no tumor development after re-implantation (PDX70, PDX189) or absence of human tumor cells in PDX (PDX30). Ultimately, 15 PDX models were included for *in vivo* determination of PARPi sensitivity and further *ex vivo* analyses (highlighted in Table 1).

PARPi response in relation to BRCA1/2 status or levels of genomic instability

The selected 15 ovarian cancer PDX models were treated for 28 days with olaparib or a solvent control treatment. In total, 8 out of 15 models showed a response to olaparib, as defined as a 30% lower mean tumor volume at the end of treatment in the olaparib-treated group versus the mean tumor growth in the control-treated group (Figure 1A and Table 1). As expected, both PDX models with CNA profile A and lacking *BRCA1/2* alterations (PDX68 and PDX112), did not respond to olaparib (Figure 1A and B). For models categorized as genomically unstable (CNA profiles D and E), 8 responded to olaparib, whereas 4 did not (Figure 1A and B). Of the five PDX models with *BRCA1/2* alterations, 1 model (PDX81) did not respond to olaparib, likely explained by its endometrioid subtype, lack of *BRCA1* LOH, and a corresponding low level of genomic instability (CNA profile A), in line with this model being MSI-high (MSI-H, Table 1). Tumor growth curves and final tumor growth percentages upon olaparib or control treatment for individual PDX models can be found in Supplementary Figure S2 and S3.

Previously, *BRCA1/2* mutational status was shown to be associated with olaparib response in breast cancer and ovarian cancer patients (13,59). Analysis of tumor responses to olaparib versus *BRCA1/2* mutation status showed that *BRCA1/2* mutational status alone was not sufficient to predict responses to olaparib (Figure 1C), with some *BRCA1/2* mutant models not responding to treatment (i.e. PDX81), whereas olaparib-sensitive models also included *BRCA1/2* wt tumors (PDX37, PDX176, PDX67, PDX174) (Figure 1C). We next assessed if the level of genomic instability was associated with response to olaparib. Whereas all three PDX models with profile A did not respond to olaparib, 8/12 models with CNA profile D or E responded to olaparib (Figure 1D), underscoring that CNA profiles are not sufficient to separate olaparib-sensitive from olaparib-insensitive models (Figure 1D). For diagnostic purposes in breast cancer, a *BRCA1* and *BRCA2* classifier was developed to identify tumors with a '*BRCA1*-like' or '*BRCA2*-like' phenotype (60). Application of the ovarian adjusted *BRCA1/2* classifiers to our selected ovarian PDX models, identified 10 out of 15 models as a '*BRCA1*- or *BRCA2*-like' tumor (Table 1). However, 3 of these 10 '*BRCA1/2*-like' models (i.e. PDX56, PDX143, PDX191) did not respond to olaparib, whereas 1 PDX model (PDX176) was not identified as '*BRCA1/2*-like' but did respond to olaparib (Figure 1E). Combined, these data show that neither the presence of a genomic *BRCA1/2* alteration, nor CNA levels or BRCA1/2-like classifier scores adequately predicted response to olaparib in this cohort of ovarian cancer models.

Functional assessment of DNA repair in relation to olaparib response in ovarian cancer PDX models

To test whether the functionality of DNA repair is associated with a response to olaparib, we analyzed two genome maintenance functions that have been attributed to BRCA1 and BRCA2, specifically the ability to recruit RAD51 to sites of DNA damage (42), and the ability to protect stalled replication forks (6,7).First, we conducted the RECAP (REpair CAPacity) assay, in which the ability of cells is assessed to recruit the downstream HR repair component RAD51 to irradiation-induced DNA damage foci (42,44). RAD51 foci formation has been previously used to identify HRD tumors and was previously shown to be associated with treatment response (61,62). Freshly isolated PDX tumor tissue from 15 models was irradiated *ex vivo* and the formation of RAD51 foci was subsequently visualized using immunofluorescence (Figure 2A and B and Table 1). Because HR is only employed in proliferating cells, the cell cycle-regulated protein geminin (GMMN) was included as a marker for S/G2 cells. Approximately 7 out of 15 PDX models showed RECAP positivity, as judged by at least 20% of geminin-positive cells showing RAD51 foci (Figure 2C). We observed a statistically significant relation between RECAP positivity and response to olaparib, with RECAP-negative tumors showing a decrease in tumor size upon treatment ($P = 0.0002$, Figure 2D). Also, when percentages of RAD51-positive tumor cells were used as a continuous variable, a strong correlation was observed between HR repair capacity and response to olaparib ($r = 0.8247$, $P = 0.002$, Figure 2E).

The ability of cells to protect their replication forks is also relevant for PARPi sensitivity, as trapping of PARP onto DNA by PARPi results into replication fork stalling (63). Therefore, we analyzed the ability of tumor cells to protect stalled replication forks, which has been shown to depend on various HR proteins and was reported to be related to olaparib response (6,16). Replication kinetics and the ability of cells to protect stalled replication forks can be assessed with the fiber technique. To this end, we were able to successfully perform *ex vivo* DNA fiber analysis on freshly isolated tumor tissue of 13/15 PDX models. Tumor tissue was dissociated into single cells and subsequently incubated with synthetic nucleotides CIdU and IdU (Figure 3A). To deplete the nucleotide pool and stall replication forks, cells were then treated with a high dose of HU. Finally, DNA was isolated and spread onto glass slides, and the incorporated synthetic nucleotides were visualized to quantify the length of replication tracts within DNA fibers. To confirm that measured fibers were originating from tumor cells, dissociated cells used for fiber analysis were simultaneously incubated with EdU to identify proliferating cells and stained for cytokeratin to identify tumor cells. For 10 PDX models, the percentage of

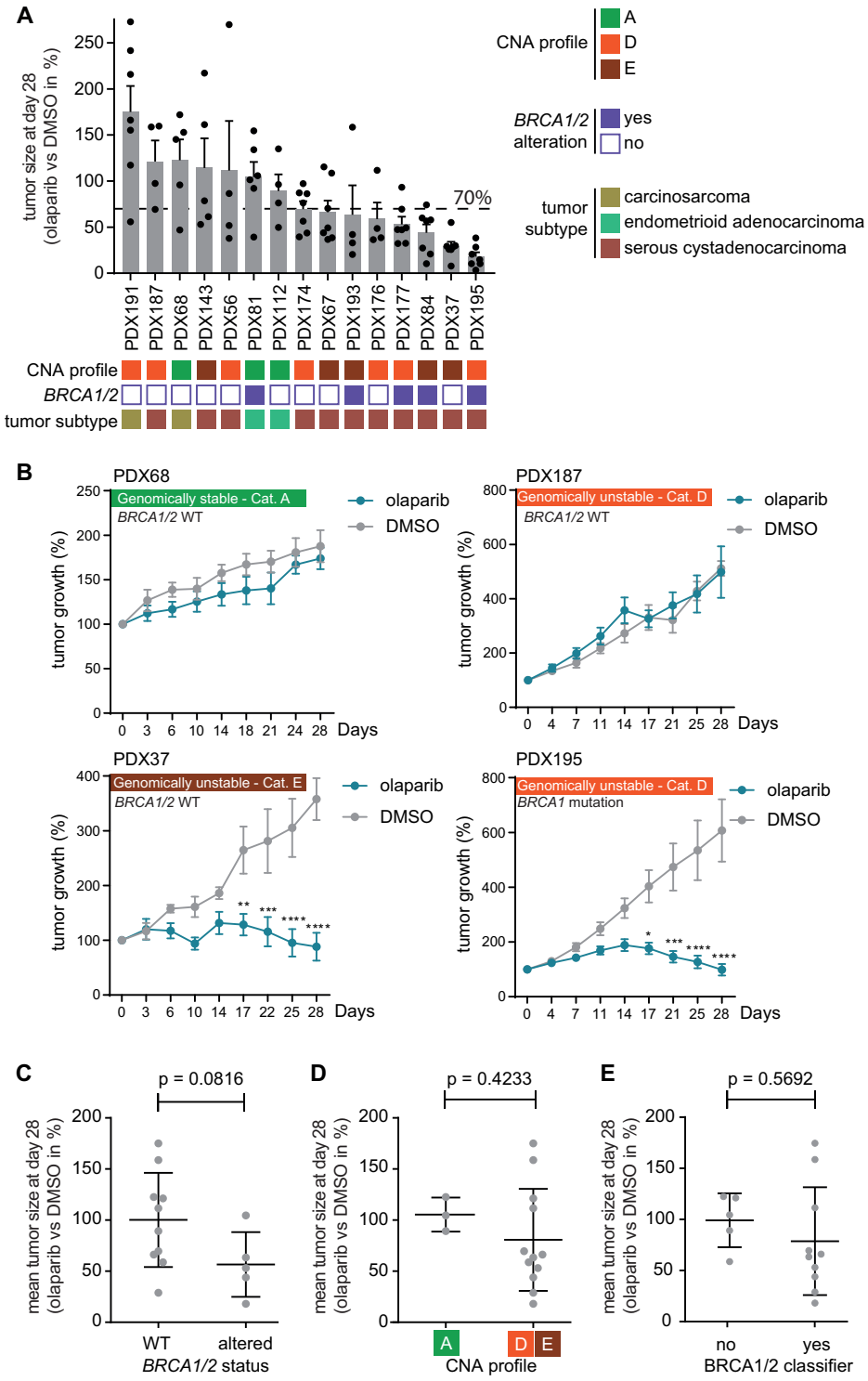

Figure 1. Response to olaparib in BRCA1/2 mutant/defective or genomically instable ovarian PDX models. (**A**) Mice were treated for 28 days with olaparib or solvent (DMSO). Bars show the mean tumor size at day 28 in the olaparib-treated group relative to the mean tumor size at day 28 in the solvent-treated group. Each dot represents one olaparib-treated mouse ($n \geq 4$). Data are shown as mean ± SEM of olaparib-treated mice. Boxes show characteristics of each PDX model. (**B**) Representative tumor growth curves of individual PDX models treated with olaparib (blue) or solvent (gray). Percentages of tumor growth were calculated as tumor volume at day *x* compared to tumor volume at day 0. Data are shown as mean ± SEM of at least 4 mice per group. *P*-values were calculated using two-way ANOVA with Bonferroni correction; $*P < 0.05$, $**P < 0.01$ and $***P < 0.001$. (**C**) Mean tumor size at day 28 in olaparib-treated mice was normalized to mean tumor size in solvent-treated mice as a measure of olaparib response (<100%). Every dot represents mean response one PDX model. *BRCA1/2* wt PDX models were separated from PDX models with a *BRCA1/2* alteration. Data are shown as mean ± SD of individual PDX models. *P*-value was calculated using two-tailed Student's t-test. (**D**) Olaparib response was calculated as described for panel (C). Each dot represents one PDX model. PDX models with CNA profile A were separated from PDX models with CNA profile D or E. Data are shown as mean ± SD of different PDX models. *P*-value was calculated using two-tailed Student's t-test. (**E**) Olaparib response was calculated as described for panel (C). Each dot represents one PDX model. PDX models classified as 'BRCA1-like' were separated from non-'BRCA1-like' tumors based on BRCA1-classifier outcome. Data are shown as mean ± SD of different PDX models. *P*-value was calculated using two-tailed Student's t-test.

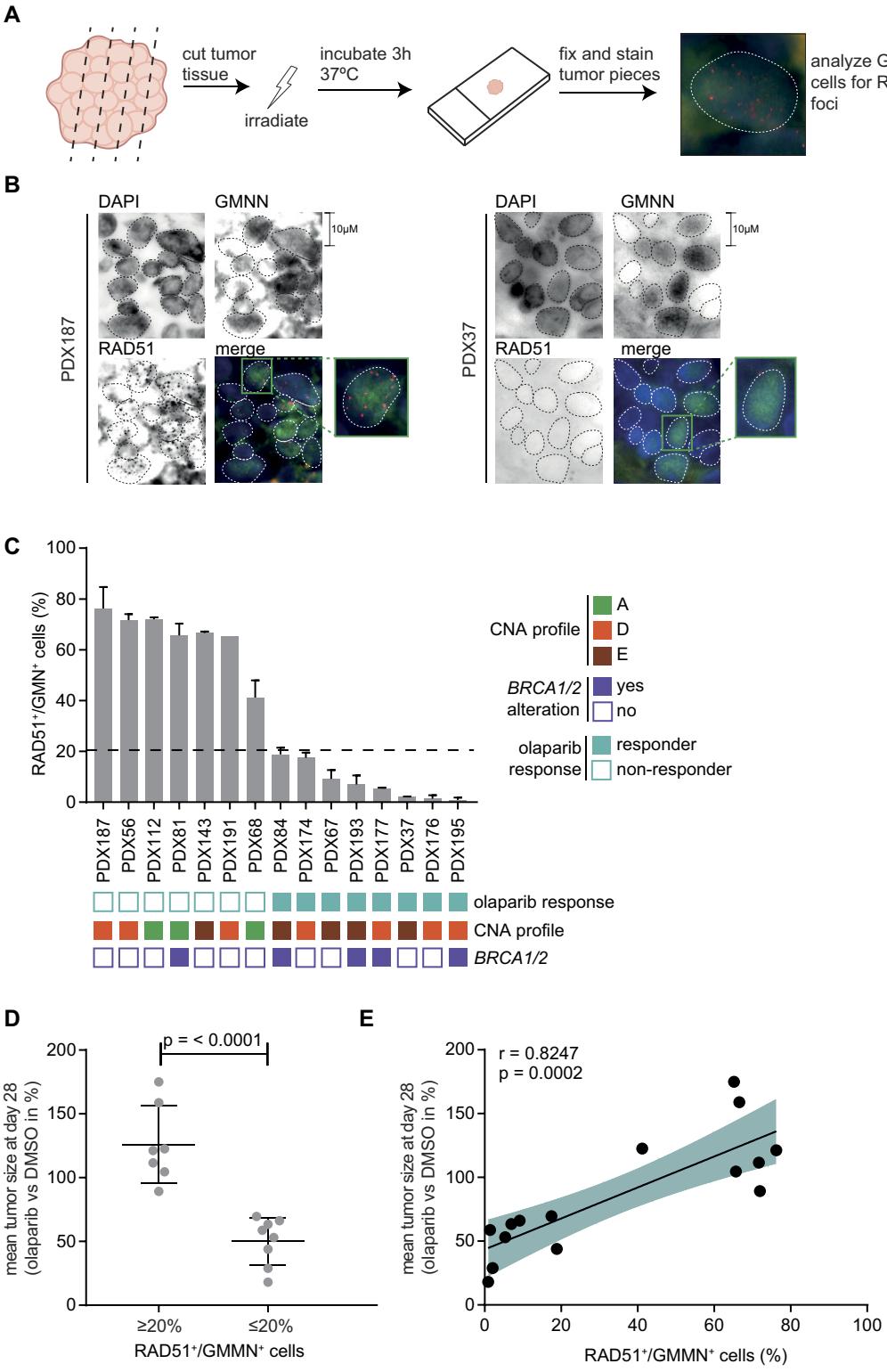

Figure 2. RECAP assay predicts olaparib response in ovarian PDX models. (**A**) Schematic workflow of the RECAP assay. Freshly isolated PDX tumor tissue was cut into small pieces and *ex vivo* irradiated with 5 Gy. Tumor pieces were incubated for 3h at 37°C and subsequently fixed, stained for RAD51 and Geminin, and microscopically analyzed. Amounts of Geminin$^+$ cells with ≥5 RAD51 foci were assessed. (**B**) Representative images of RAD51/Geminin staining of irradiated tumor tissue of PDX187 (RAD51$^+$, HR proficient) and PDX37 (RAD51$^-$, HRD). (**C**) Bars represent percentages of RAD51$^+$/Geminin$^+$ cells of individual PDX models. The dotted line marks the threshold of ≤ 20% Rad51$^+$/Geminin$^+$ cells, indicating HR deficiency. Boxes show different characteristics of each PDX model. Data are shown as mean ± SEM of at least three different tissue slides. (**D**) Olaparib response was plotted as mean tumor size at day 28 in olaparib-treated mice normalized to mean tumor size in solvent-treated mice. Each dot represents one PDX model. HR proficient (>20% Rad51$^+$/Geminin$^+$ cells) PDX models were separated from HRD (≤20% Rad51$^+$/Geminin$^+$ cells) PDX models. Data are shown as mean ± SD of different PDX models. *P*-value was calculated using two-tailed Student's t-test. (**E**) Percentages of RAD51$^+$/Geminin$^+$ cells and mean percentages of tumor growth from olaparib-treated mice versus solvent-treated mice were plotted. Each dot represents one PDX model. Correlation coefficients were calculated using Pearson, and linear regression was plotted.

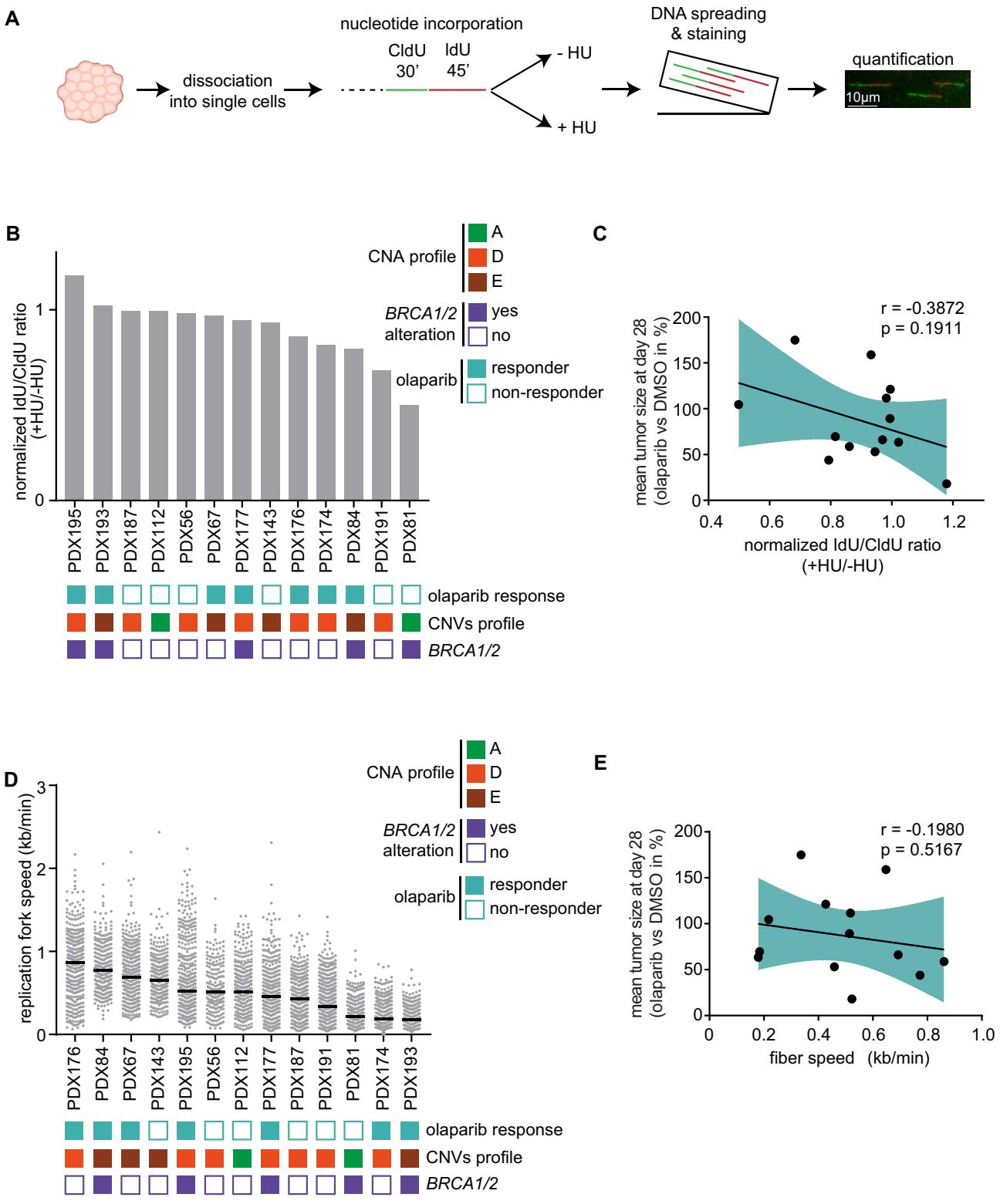

Figure 3. Analysis of replication fork stability and replication speed does not correlate with olaparib responses in ovarian PDX models. (**A**) Schematic workflow of *ex vivo* DNA fiber analysis. Freshly isolated tumor tissue was dissociated into single cells and incubated with synthetic nucleotides CldU and IdU. Cells were subsequently treated with or without HU to stall replication forks. DNA was then isolated, stretched and fixed onto glass slides. Incorporated synthetic nucleotides were visualized, and length of DNA fibers was quantified. (**B**) The ratio of IdU/CldU fiber lengths upon HU treatment were normalized to the untreated condition. Bars represent normalized ratios per PDX model. A ratio of <1 (dotted line) represents replication fork degradation. Boxes indicate different characteristics of each PDX model. (**C**) Normalized IdU/ClDU ratios and mean percentages of tumor growth from olaparib-treated mice versus solvent-treated mice were plotted. Each dot represents one PDX model. Correlation coefficients were calculated using Pearson and linear regression was plotted. (**D**) Replication fork speed (kb/min) of CldU fibers was calculated as mentioned in the methods. Data are shown as median of all measured fibers per PDX. Each dot represents one fiber. Boxes indicate different characteristics of each PDX model as for panel (B). (**E**) Median fiber speed and mean percentages of tumor growth from olaparib-treated mice versus solvent-treated mice were plotted. Each dot represents one PDX model. Correlation coefficients were calculated using Pearson and linear regression was plotted.

Edu-positive cells that were also cytokeratin-positive were analyzed, which the proliferating cells almost exclusively reflected tumor cells (Supplementary Figure S4A and B). As a readout for the ability of tumor cells to protect replication forks from HU-induced degradation, IdU/CldU ratios in HU-treated cells were normalized to the untreated setting, with a value of 1 reflecting fully protected replication forks, and a value of 0 reflecting no fork protection (Figure 3B, with all individual IdU/CldU ratios in -HU and + HU conditions in Supplementary Figure S4C). A substantial range in the ability to protect replication forks was observed between PDX models (Figure 3B). Surprisingly, PDX81 showed the lowest degree of replication fork protection, but had a heterozygous *BRCA1* deletion and was classified as genomically stable (CNA profile A) (Figure 3B), whereas PDX195 and PDX193 showed defective HR as judged by loss of RAD51 recruitment, were genomically instable (CAN profile D and E) respectively, and harbored *BRCA1* gene mutations, but did not show a fork protection defect. When normalized IdU/CldU ratios were used as a continuous variable, a slight negative relation between replication fork protection and response to olaparib was observed ($r = -0.3872$), which was not statistically significant ($P = 0.1911$, Figure 3C). As an additional readout for replication stress, we calculated the overall replication speed (Figure 3D). Similar to normalized IdU/CldU ratios (Figure 3B and C), analysis of overall replication speed showed a substantial degree of variation between PDX models and did not show an association with CNA profiles or *BRCA1/2* mutation status (Figure 3D and E). Also, overall replication speed was not correlated with response to olaparib ($r = -0.1980$, $P = 0.5167$, Figure 3E).

Despite the low number of PDX models compared to clinical studies, 'receiver operating characteristic' (ROC) curves from genomic (Supplementary Figure S4D) and functional analyses (Supplementary Figure S4E) demonstrated that the RECAP assay could predict *in vivo* olaparib response with an AUC of 1. Additionally, the optimal cut-off value of the RECAP result (between 18.15 and 30.02%) determined by the ROC curve confirms our 20% cut-off used that was previously determined (42). Thus, in contrast to replication fork protection or replication speed, a functional read-out of HR repair capacity based on RAD51 recruitment was associated with response to olaparib in this cohort of ovarian cancer PDX models.

Mutations in olaparib-sensitive PDX model

Since a number of PDX models showed response to olaparib that could not be explained by *BRCA1/2* alterations, we analyzed a panel of 226 genes that were previously demonstrated to be involved in DNA repair (Supplementary Table S1). Panel sequencing was performed on 10 PDX models (indicated in Table 1), including olaparib-sensitive PDX models without *BRCA1/2* alterations. Candidate variants were filtered for germline variant frequencies found in patients and controls. Concordant with our first genomic DNA analyses, all *BRCA1/2* mutations were identified in PDX81, PDX177, PDX189 and PDX195 (Table 2). Besides the identified *BRCA1/2* variants, 19 additional variants were identified in olaparib-sensitive models (Table 2). Furthermore, 7/10 models showed mutated *TP53* and two out of three *TP53* wt samples had inactivated *PTEN* and mutant *MSH2/3* (data not shown). PDX112 did not harbor any of these alterations and was also sequenced as a *BRCA1/2* wt control model with CNA profile A.

One particular variant in the olaparib-sensitive, *BRCA1/2* wt PDX37 caught our attention; a single-nucleotide variant (SNV) in *MUS81*, altering arginine on position 496 to glutamine (R496Q, highlighted in Table 2). The underlying c.1487G > A mutation was homozygous, and resides in a highly conserved region close to the ERCC4 binding domain, within a predicted Hef domain (Figure 4A and B). Furthermore, *MUS81* loss has previously been shown to cause olaparib sensitivity, including in genome-wide CRISPR screens and was shown to cause olaparib sensitivity when depleted in ovarian cancer cell lines (64,65). Using U2OS cells, we could confirm that MUS81 inactivation leads to sensitivity to olaparib and cisplatin (Supplementary Figure S5A and B), albeit without loss of RAD51 foci formation capacity. To test the effect of R496Q-MUS81 on PARPi sensitivity, we used eHAP1 MUS81 knockout cells (Figure 4C), which were transduced with wt-MUS81 or R496Q-MUS81 (Figure 4C). As expected, sHAP1 *MUS81*^{KO} cells showed increased olaparib sensitivity, which was largely rescued by expression of wt-MUS81 (Figure 4D). In contrast, expression of R496Q-MUS81 only showed a partial rescue of olaparib sensitivity (Figure 4D). Of note, the expression levels of R496Q-MUS81 were slightly lower than those of wt-MUS81, possibly pointing toward R496Q-MUS81 being less stable.

Discussion

In this study, we associated *in vivo* olaparib PARPi responses to genomic features related to HRD, functional HR assessment and replication fork stability in a cohort of ovarian cancer PDX models. Although RAD51 foci formation has been previously described as a tool to identify HRD tumors, and has been studied in relation to treatment response, to our knowledge, this is the first study in which both RAD51 formation and replication fork protection is analyzed in relation to *in vivo* PARPi response in patient-derived models of ovarian cancer. In our cohort of ovarian cancer PDX models, the presence of *BRCA1/2* alterations, including *BRCA1* promoter methylation, was not significantly associated with *in vivo* olaparib response in the tested cohort of PDX models. Also, only a subset of genomically unstable tumors, as assessed by CNA analysis, responded to olaparib. These findings underscored the need for alternative or additional selection methods for PARPi eligibility. Functional testing of replication fork stability or replication speed using DNA fiber analysis on freshly isolated tumor tissue did not correlate to *in vivo* olaparib responses. In contrast, the RECAP assay, which tests HR functionality as determined by the formation of RAD51 foci in *ex vivo* tumor tissue, fully predicted *in vivo* olaparib response. Several PDX models were identified that were defective for RAD51 foci formation and were responsive to PARPi, while they did not harbor *BRCA1/2* alterations. These results further support the use of the RECAP method to identify patients that may benefit from PARPi, beyond those with *BRCA1/2* mutant tumors.

Clinical trials previously demonstrated that PARPi can be beneficial in patients with breast or ovarian cancers lacking *BRCA1/2* mutations (33,41), and other cancer types (66). So, there is a clear need for a robust biomarker of HR functionality that correlates with PARPi response. To this end, various HRD tests have been developed, focused mostly on ge-

Table 2. Variants found with panel sequencing in PARPi sensitive PDX models

PDX #	sample # (see table 1)	Chromosome	Gene	Alteration	het/hom	Exogenic function
37	S01	chr10	DMBT1	DMBT1:NM_007 329:exon17: c.1975C > T:p.Q659X	hom	Stopgain SNV
37	S01	chr11	MUS81	MUS81:NM_025 128:exon14: c.1487G > A:p.R496Q	hom	Nonsynonymous SNV
37	S01	chr5	TERT	TERT:NM_198 253:exon2: c.1171C > T:p.P391S	het	Nonsynonymous SNV
37	S01	chr9	TLR4	TLR4:NM_138 554:exon2:c.T197A:p.L66Q, TLR4:NM_003 266:exon3:c.T77A:p.L26Q	het	Nonsynonymous SNV
37	S01	chr17	TP53	TP53:NM_000 546:exon7: c.742C > T:p.R248W	hom	Nonsynonymous SNV
37	S01	chr10	ZNF365	ZNF365:NM_014 951:exon5: c.1093G > A:p.E365K	het	Nonsynonymous SNV
67	S02	chr7	EGFR	EGFR:NM_201 284:exon16: c.2060G > A:p.S687N	het	Nonsynonymous SNV
67	S02	chr8	PREX2	PREX2:NM_024 870:exon17: c.1876G > A:p.E626K	het	Nonsynonymous SNV
67	S02	chr17	TP53	TP53:NM_000 546:exon8: c.844C > T:p.R282W	hom	Nonsynonymous SNV
81	S03	chr17	BRCA1	BRCA1:NM_007 294:exon10: c.1823delA:p.K608fs	het	Frameshift deletion
174	S05	chr11	CWF19L2	CWF19L2:NM_152 434:exon3: c.273delA:p.K91fs	het	Frameshift deletion
174	S05	chr10	DMBT1	DMBT1:NM_007 329:exon26: c.2975C > T:p.A992V	het	Nonsynonymous SNV
174	S05	chr9	TLR4	TLR4:NM_003 266:exon4: c.1402C > A:p.L468M	het	Nonsynonymous SNV
174	S05	chr17	TP53	TP53:NM_000 546:exon9: c.972dupT:p.G325fs	hom	Frameshift insertion
176	S06	chr11	CDKN1C	CDKN1C:NM_000 076:exon1: c.549_554del:p.183_185del	hom	Nonframeshift deletion
176	S06	chr10	FAM175B	FAM175B:NM_032 182:exon9: c.1120G > A:p.D374N	het	Nonsynonymous SNV
176	S06	chr17	TP53	TP53:NM_000 546:exon5: c.488A > G:p.Y163C	hom	Nonsynonymous SNV
177	S07	chr13	BRCA2	BRCA2:NM_000 059:exon10: c.1457delA:p.Q486fs	hom	Frameshift deletion
177	S07	chr17	TP53	TP53:NM_000 546:exon8: c.817C > T:p.R273C	hom	Nonsynonymous SNV
189	S08	chr13	BRCA2	BRCA2:NM_000 059:exon23: c.9090delA:p.T3030fs	het	Frameshift deletion
193	S09	chr16	AXIN1	AXIN1:NM_003 502:exon2: c.833C > T:p.P278L	het	Nonsynonymous SNV
193	S09	chr13	ERCC5	ERCC5:NM_000 123:exon15: c.3356C > T:p.A1119V	het	Nonsynonymous SNV
193	S09	chr17	TP53	TP53:NM_000 546:exon7: c.737T > C:p.M246T	hom	Nonsynonymous SNV
195	S10	chr17	BRCA1	BRCA1:NM_007 294:exon23: c.5542delC:p.Q1848fs	het	Frameshift deletion

nomic features. The myChoice HRD test combines *BRCA1/2* mutation status with different measurements of genomic instability, but was unable to predict responses to the PARPi niraparib in ovarian cancer (33). HRDetect is based on algorithms on whole-genome sequencing profiles from *BRCA1/2*-mutated breast cancers and was able to detect HRD tumors that responded to platinum-based chemotherapy (34). Reported studies in which HRDetect is used to predict responses to PARPis are still lacking.

Despite the fact that these genomic analyses are relatively easily applicable in the clinic, they do not reflect HR functionality at time of treatment decision making. This is relevant, because functionality of the HR pathway can be restored in *BRCA1/2* mutant tumors through secondary mutations which cause PARPi resistance (30,37). Such mutations can arise due to previous treatments with DNA damaging agents such as chemotherapy or during PARPi treatment (67).

Our findings are in line with other reports, in which functional testing of HR by RAD51 foci formation is able to detect HR deficiency in breast cancer (44). The RECAP assay was used in an extensive cohort of primary breast cancer tissues ($n = 148$) and identified 19% of these samples to be HRD, of which seven samples were non-*BRCA1/2*-related (44). In this latter study, however, correlation with clinical treatment response was lacking.

The relevance of assessing HR functionality by detection of RAD51 foci was underscored in *BRCA1/2*-mutated breast cancer PDX models, in which HR function was restored and therefore caused PARPi resistance (46). Importantly, the RECAP assay was able to identify HR restoration, despite various underlying mechanisms. Also, the RECAP assay was able to detect restoration of HR in *BRCA1* mutant metastatic breast cancer upon treatment with platinum-based and PARPi treatment (47).

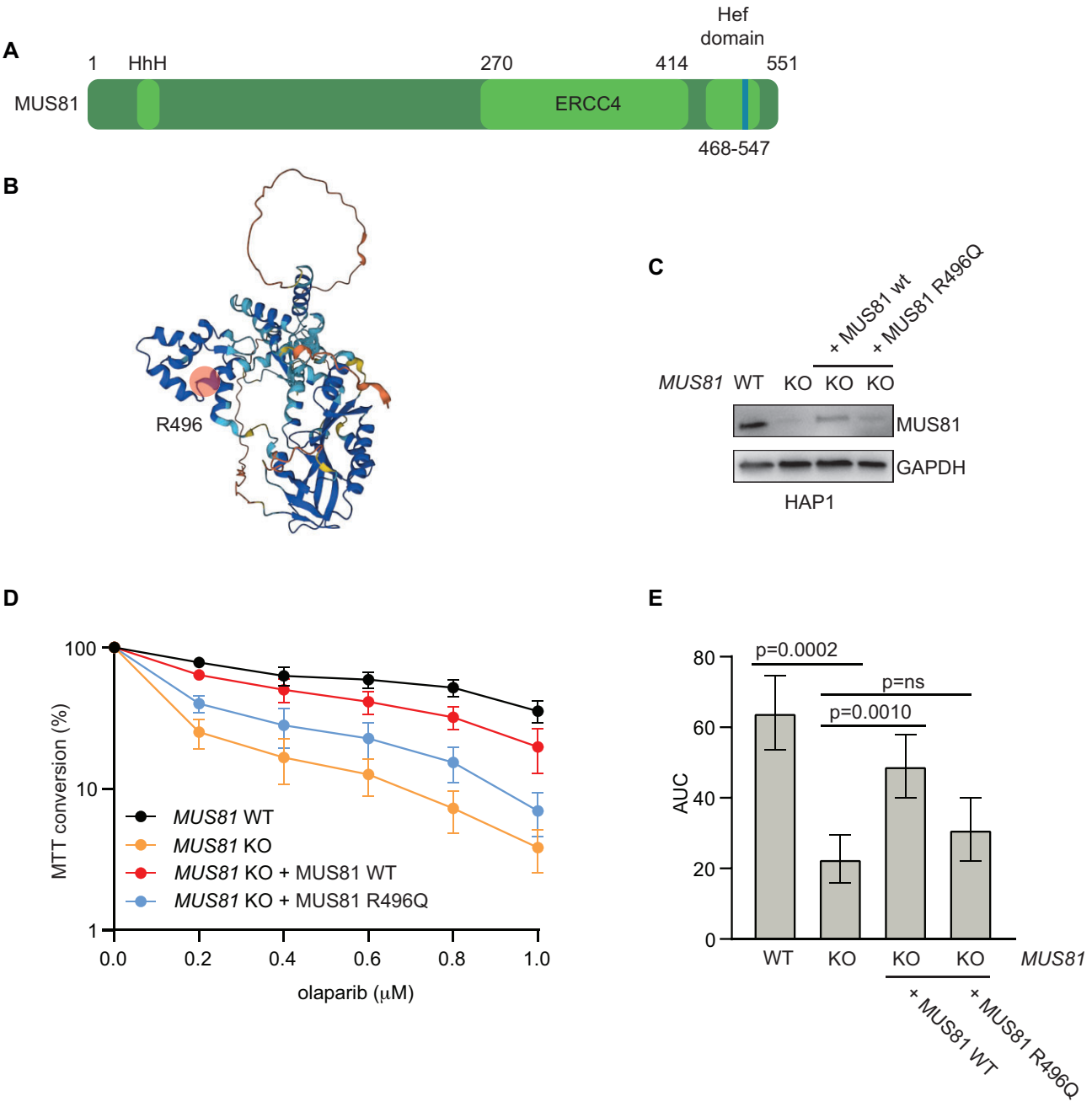

Figure 4. Analysis of MUS81 R496Q variant in the context of PARPi sensitivity. (**A** and **B**) Schematic depiction of functional domains (A) and structure of MUS81 (B) with R498 located in the Hef domain at the surface of the protein. (**C**) Immunoblot analysis of eHAP *MUS81*^{wt}, *MUS81*^{KO} and eHAP *MUS81*^{KO} reconstituted with MUS81^{WT} or MUS81^{R498Q}. Immunoblot shows MUS81 and GAPDH protein levels. (**D**) eHAP cells described in C cells were treated with indicated concentration of olaparib. Percentages of surviving cells were measured by MTT. Data are presented as mean ± SEM of five replicates. (**E**) Quantification of AUC of cells treated as described in (D). *P*-values were calculated using a Student's t-test

In the RECAP assay, the formation of RAD51 foci is assessed by immunofluorescence upon *ex vivo* irradiation. Although this creates a good dynamic window to detect HR defects, it comes with logistic challenges, including the processing of fresh tumor tissue and the availability of a radiation source. Interestingly, recent studies analyzed endogenous RAD51 foci in untreated paraffin-embedded samples. In this approach, RAD51 assessment was successful in identifying olaparib-sensitive breast cancer PDX models, beyond *BRCA1/2* mutated tumors (45). Whether this approach is also feasible for ovarian cancer tissues remains unclear.

Of note, PARPi resistance might also occur independently of HR restoration, involving restored replication fork protection (16) or suppression of ssDNA gaps (19). However, using non-transformed human epithelial cell lines, primarily the role of BRCA2 in HR was responsible for maintaining cell viability and prevention of replication stress, and not its role in replication fork protection (68). Moreover, the role of BRCA2 in HR, but not fork stabilization or ssDNA gap suppression was recently shown to determine PARPi sensitivity in genetically engineered mouse models with separation-of-function *Brca2* mutants (29). In line with these findings in engineered systems,

in our PDX cohort the HR capability of tumor cells but not the ability to protect replication forks was associated with *in vivo* olaparib response.

Interestingly, two PDX models (PDX81, PDX189), with a *BRCA1* and *BRCA2* mutation respectively, were classified as genomically stable, as based on CNA profile (profile A and B) and did not show BRCAness based on *BRCA1/2*-like scores (score 0.00 for *BRCA1*-like and 0.07 and 0.09 for *BRCA2*-like, respectively). Furthermore, PDX81 did not respond to olaparib *in vivo*. The observation that these PDX models did not behave as 'BRCAness' tumors, might partially be explained by these tumors being derived from primary endometrioid ovarian tumors. Furthermore, the identified *BRCA1/2* mutations had an allele frequency of approximately 50%, suggesting that these are heterozygous mutations without LOH. Finally, both tumors were classified as MSI-high, caused by *MLH1* promoter methylation in one model (PDX189). This may have resulted in the presence of a heterozygous *BRCA1/2* mutation as a passenger mutation, without a BRCAness phenotype. Unfortunately, PDX189 was not available for *in vivo* olaparib response analysis. For PDX181, no underlying cause of MSI was identified.

We finally aimed to find the underlying cause of HRD in PDX models sensitive to olaparib without harboring a *BRCA1/2* alteration ($n = 4$). We identified several interesting homozygous mutations in olaparib-sensitive PDX models, as a possible mechanism underlying HRD. We identified a variant in *MUS81*, which was not able to rescue PARPi sensitivity when compared to wt *MUS81*. However, loss of MUS81 did not interfere with RAD51 recruitment, making it unclear if the *MUS81* variant in PDX37 is responsible for olaparib sensitivity, while also indicating that additional defects in PDX37 are responsible for the RAD51 defect. Moreover, the slightly lower expression level of R496Q-MUS81 may indicate this this variant is less stable at the protein level. Future research into *MUS81* variants, and analysis of other genomic aberrancies is warranted to reveal which mutations underlie HR deficiency and olaparib sensitivity in these models.

In summary, we showed that functional testing of HR with the RECAP assay correlates to *in vivo* olaparib response in a cohort of ovarian cancer PDX models. Surprisingly, the presence of *BRCA1/2* alterations, CNA profile or *ex vivo* assessed replication fork protection did not correlate to *in vivo* olaparib response in ovarian cancer PDX models. Several PDX models were identified as HRD and PARPi sensitive without carrying a *BRCA1/2* alteration. The RECAP assay warrants further investigation in clinical trials to assess its predictive potential for *in vivo* response to PARPi therapy to increase the population of patients that might benefit from PARPi therapy.

Limitation of the study

This study has limitations. First, we only correlated *in vivo* PARPi sensitivity of PDX models to HR function and replication fork stability analysis. We did not analyze ssDNA gaps, a recently identified mechanisms of PARPi sensitivity in BRCA1/2 mutant cancer cells. Therefore, in the current study we cannot draw conclusions on how ssDNA gap determination would perform in comparison to HR functionality in predicting PARPi response. Second, analysis of replication fork velocity in PDX material showed significant variation within tumor samples, which we previously also observed in DNA fiber analysis of primary breast cancer tissues (69). Using patient-derived tumor tissues, iso-genic controls are lacking to determine a threshold for defective replication fork protection, which may negatively impact the interpretability of these assays. Thirdly, we identified a *MUS81* variant in PDX37, which conferred partial PARPi sensitivity when introduced in a cell line model. However, loss of MUS81 does not lead to a defect in RAD51 loading, indicating that the MUS81 variant is not responsible for all phenotypes of PDX37.

Data availability

The data underlying this article will be shared on reasonable request to the corresponding author.

Supplementary data

Supplementary Data are available at NAR Cancer Online.

Acknowledgements

Author contributions: M.A.T.M.v.V. and F.T. conceived and initiated the project. F.T. and V.O.N.T. performed *in vivo* and *ex vivo* experiments. E.H.R., P.M.N. and R.D.D. performed genomic *BRCA1/2* and CNV analyses. M.J., P.Z. and Z.K. performed targeted DNA sequencing. S.d.J. and G.B.A.W. established and provided PDX models. E.W.D. analyzed H&E stainings from PDX tumors. F.T., V.O.N.T., E.H.R., P.M.N., M.J., P.Z., Z.K. and M.A.T.M.v.V. analyzed data. F.T. and M.A.T.M.v.V. wrote the manuscript. All authors provided feedback on the manuscript before submission. We thank Frans Hogervorst and Rob Plug for technical support; Stephen West and Kasper Fugger for sharing reagents; members of the Medical Oncology Department for discussions and feedback on the manuscript; and Marta Kalousova and Marketa Safarikova for providing technological capacity for NGS analyses.

Funding

The Dutch Cancer Society [2014–7048 to M.A.T.M.v.V.], MZ CR NU20-03-00016, RVO-VFN64165, MSMT CR LX22NPO5102] to Charles University.

Conflict of interest statement

M.A.T.M.v.V. has acted on the Scientific Advisory Boards of Nodus Oncology and RepareTx, unrelated to this work. All other authors declare no competing.

References

1. Reid,B.M., Permuth,J.B. and Sellers,T.A. (2017) Epidemiology of ovarian cancer: a review. *Cancer Biol. Med.*, **14**, 9–32.
2. Cancer Genome Atlas Research Network, Bell,D., Berchuck,A., Birrer,M., Chien,J., Cramer,D.W., Dao,F., Dhir,R., Disaia,P., Gabra,H., *et al.* (2011) Integrated genomic analyses of ovarian carcinoma. *Nature*, **474**, 609–615.
3. Antoniou,A., Pharoah,P.D.P., Narod,S., Risch,H.A., Eyfjord,J.E., Hopper,J.L., Loman,N., Olsson,H., Johannsson,O., Borg,Å., *et al.* (2003) Average risks of breast and ovarian cancer associated with BRCA1 or BRCA2 mutations detected in case series unselected for family history: a combined analysis of 22 studies. *Am. J. Hum. Genet.*, **72**, 1117–1130.

4. Kuchenbaecker,K.B., Hopper,J.L., Barnes,D.R., Phillips,K.A., Mooij,T.M., Roos-Blom,M.J., Jervis,S., Van Leeuwen,F.E., Milne,R.L., Andrieu,N., *et al.* (2017) Risks of breast, ovarian, and contralateral breast cancer for BRCA1 and BRCA2 mutation carriers. *J. Am. Med. Assoc.*, **317**, 2402–2416.
5. Moynahan,M.E. and Jasin,M. (2010) Mitotic homologous recombination maintains genomic stability. *Nat. Rev. Mol. Cell Biol.*, **11**, 196–207.
6. Schlacher,K., Wu,H. and Jasin,M. (2012) A distinct replication fork protection pathway connects fanconi anemia tumor suppressors to RAD51-BRCA1/2. *Cancer Cell*, **22**, 106–116.
7. Schlacher,K., Christ,N., Siaud,N., Egashira,A., Wu,H. and Jasin,M. (2011) Double-strand break repair-independent role for BRCA2 in blocking stalled replication fork degradation by MRE11. *Cell*, **145**, 529–542.
8. Cong,K., Peng,M., Kousholt,A.N., Lee,W.T.C., Lee,S., Nayak,S., Krais,J., VanderVere-Carozza,P.S., Pawelczak,K.S., Calvo,J., *et al.* (2021) Replication gaps are a key determinant of PARP inhibitor synthetic lethality with BRCA deficiency. *Mol. Cell*, **81**, 3128–3144.
9. Kang,Z., Fu,P., Alcivar,A.L., Fu,H., Redon,C., Foo,T.K., Zuo,Y., Ye,C., Baxley,R., Madireddy,A., *et al.* (2021) BRCA2 associates with MCM10 to suppress PRIMPOL-mediated repriming and single-stranded gap formation after DNA damage. *Nat. Commun.*, **12**, 5966.
10. Taglialatela,A., Leuzzi,G., Sannino,V., Cuella-Martin,R., Huang,J.-W., Wu-Baer,F., Baer,R., Costanzo,V. and Ciccia,A. (2021) REV1-Polζ maintains the viability of homologous recombination-deficient cancer cells through mutagenic repair of PRIMPOL-dependent ssDNA gaps. *Mol. Cell*, **81**, 4008–4025.
11. Bryant,H.E., Schultz,N., Thomas,H.D., Parker,K.M., Flower,D., Lopez,E., Kyle,S., Meuth,M., Curtin,N.J. and Helleday,T. (2005) Specific killing of BRCA2-deficient tumours with inhibitors of poly(ADP-ribose) polymerase. *Nature*, **434**, 913–917.
12. Farmer,H., McCabe,H., Lord,C.J., Tutt,A.H.J., Johnson,D.A., Richardson,T.B., Santarosa,M., Dillon,K.J., Hickson,I., Knights,C., *et al.* (2005) Targeting the DNA repair defect in BRCA mutant cells as a therapeutic strategy. *Nature*, **434**, 917–921.
13. Robson,M., Im,S.A., Senkus,E., Xu,B., Domchek,S.M., Masuda,N., Delaloge,S., Li,W., Tung,N., Armstrong,A., *et al.* (2017) Olaparib for metastatic breast cancer in patients with a germline BRCA mutation. *N. Engl. J. Med.*, **377**, 523–533.
14. Helleday,T. (2011) The underlying mechanism for the PARP and BRCA synthetic lethality: clearing up the misunderstandings. *Mol. Oncol.*, **5**, 387–393.
15. Murai,J., Huang,S.N.Y.N., Das,B.B., Renaud,A., Zhang,Y., Doroshow,J.H., Ji,J., Takeda,S. and Pommier,Y. (2012) Trapping of PARP1 and PARP2 by clinical PARP inhibitors. *Cancer Res.*, **72**, 5588–5599.
16. Ray Chaudhuri,A., Callen,E., Ding,X., Gogola,E., Duarte,A.A., Lee,J.-E., Wong,N., Lafarga,V., Calvo,J.A., Panzarino,N.J., *et al.* (2016) Replication fork stability confers chemoresistance in BRCA-deficient cells. *Nature*, **535**, 382–387.
17. Pommier,Y., O'Connor,M.J. and de Bono,J. (2016) Laying a trap to kill cancer cells: PARP inhibitors and their mechanisms of action. *Sci. Transl. Med.*, **8**, 362ps17.
18. Maya-Mendoza,A., Moudry,P., Merchut-Maya,J.M., Lee,M., Strauss,R. and Bartek,J. (2018) High speed of fork progression induces DNA replication stress and genomic instability. *Nature*, **559**, 279–284.
19. Cong,K., Peng,M., Kousholt,A.N., Lee,W.T.C., Lee,S., Nayak,S., Krais,J., VanderVere-Carozza,P.S., Pawelczak,K.S., Calvo,J., *et al.* (2021) Replication gaps are a key determinant of PARP inhibitor synthetic lethality with BRCA deficiency. *Mol. Cell*, **81**, 3227.
20. Panzarino,N.J., Krais,J.J., Cong,K., Peng,M., Mosqueda,M., Nayak,S.U., Bond,S.M., Calvo,J.A., Doshi,M.B., Bere,M., *et al.* (2021) Replication gaps underlie BRCA deficiency and therapy response. *Cancer Res.*, **81**, 1388–1397.
21. Petropoulos,M., Karamichali,A., Rossetti,G.G., Freudenmann,A., Iacovino,L.G., Dionellis,V.S., Sotiriou,S.K. and Halazonetis,T.D. (2024) Transcription-replication conflicts underlie sensitivity to PARP inhibitors. *Nature*, **628**, 433–441.
22. Pettitt,S.J., Frankum,J.R., Punta,M., Lise,S., Alexander,J., Chen,Y., Yap,T.A., Haider,S., Tutt,A.N.J. and Lord,C.J. (2020) Clinical BRCA1/2 reversion analysis identifies hotspot mutations and predicted neoantigens associated with therapy resistance. *Cancer Discov.*, **10**, 1475–1488.
23. Bouwman,P., Aly,A., Escandell,J.M., Pieterse,M., Bartkova,J., Van Der Gulden,H., Hiddingh,S., Thanasoula,M., Kulkarni,A., Yang,Q., *et al.* (2010) 53BP1 loss rescues BRCA1 deficiency and is associated with triple-negative and BRCA-mutated breast cancers. *Nat. Struct. Mol. Biol.*, **17**, 688–695.
24. Bunting,S.F., Callén,E., Wong,N., Chen,H.T., Polato,F., Gunn,A., Bothmer,A., Feldhahn,N., Fernandez-Capetillo,O., Cao,L., *et al.* (2010) 53BP1 inhibits homologous recombination in brca1-deficient cells by blocking resection of DNA breaks. *Cell*, **141**, 243–254.
25. Xu,G., Ross Chapman,J., Brandsma,I., Yuan,J., Mistrik,M., Bouwman,P., Bartkova,J., Gogola,E., Warmerdam,D., Barazas,M., *et al.* (2015) REV7 counteracts DNA double-strand break resection and affects PARP inhibition. *Nature*, **521**, 541–544.
26. Dev,H., Chiang,T.W.W., Lescale,C., de Krijger,I., Martin,A.G., Pilger,D., Coates,J., Sczaniecka-Clift,M., Wei,W., Ostermaier,M., *et al.* (2018) Shieldin complex promotes DNA end-joining and counters homologous recombination in BRCA1-null cells. *Nat. Cell Biol.*, **20**, 954–965.
27. Noordermeer,S.M., Adam,S., Setiaputra,D., Barazas,M., Pettitt,S.J., Ling,A.K., Olivieri,M., Álvarez-Quilón,A., Moatti,N., Zimmermann,M., *et al.* (2018) The shieldin complex mediates 53BP1-dependent DNA repair. *Nature*, **560**, 117–121.
28. Barazas,M., Annunziato,S., Pettitt,S.J., de Krijger,I., Ghezraoui,H., Roobol,S.J., Lutz,C., Frankum,J., Song,F.F., Brough,R., *et al.* (2018) The CST complex mediates end protection at double-strand breaks and promotes PARP inhibitor sensitivity in BRCA1-deficient cells. *Cell Rep.*, **23**, 2107–2118.
29. Lim,P.X., Zaman,M., Feng,W. and Jasin,M. (2024) BRCA2 promotes genomic integrity and therapy resistance primarily through its role in homology-directed repair. *Mol. Cell*, **84**, 447–462.e10.
30. Talens,F., Jalving,M., Gietema,J.A. and Van Vugt,M.A. (2017) Therapeutic targeting and patient selection for cancers with homologous recombination defects. *Exp. Opin. Drug Discov.*, **12**, 565–581.
31. Telli,M.L., Timms,K.M., Reid,J., Hennessy,B., Mills,G.B., Jensen,K.C., Szallasi,Z., Barry,W.T., Winer,E.P., Tung,N.M., *et al.* (2016) Homologous recombination deficiency (HRD) score predicts response to platinum-containing neoadjuvant chemotherapy in patients with triple-negative breast cancer. *Clin. Cancer Res.*, **22**, 3764–3773.
32. Tutt,A., Tovey,H., Cheang,M.C.U., Kernaghan,S., Kilburn,L., Gazinska,P., Owen,J., Abraham,J., Barrett,S., Barrett-Lee,P., *et al.* (2018) Carboplatin in BRCA1/2-mutated and triple-negative breast cancer BRCAness subgroups: the TNT Trial. *Nat. Med.*, **24**, 628–637.
33. Mirza,M.R., Monk,B.J., Herrstedt,J., Oza,A.M., Mahner,S., Redondo,A., Fabbro,M., Ledermann,J.A., Lorusso,D., Vergote,I., *et al.* (2016) Niraparib maintenance therapy in platinum-sensitive, recurrent ovarian cancer. *N. Engl. J. Med.*, **375**, 2154–2164.
34. Davies,H., Glodzik,D., Morganella,S., Yates,L.R., Staaf,J., Zou,X., Ramakrishna,M., Martin,S., Boyault,S., Sieuwerts,A.M., *et al.* (2017) HRDetect is a predictor of BRCA1 and BRCA2 deficiency based on mutational signatures. *Nat. Med.*, **23**, 517–525.
35. Angus,L., Smid,M., Wilting,S.M., van Riet,J., Van Hoeck,A., Nguyen,L., Nik-Zainal,S., Steenbruggen,T.G., Tjan-Heijnen,V.C.G., Labots,M., *et al.* (2019) The genomic landscape of metastatic breast cancer highlights changes in mutation and signature frequencies. *Nat. Genet.*, **51**, 1450–1458.

36. Zhao,E.Y., Shen,Y., Pleasance,E., Kasaian,K., Leelakumari,S., Jones,M., Bose,P., Ch'ng,C., Reisle,C., Eirew,P., *et al.* (2017) Homologous recombination deficiency and platinum-based therapy outcomes in advanced breast cancer. *Clin. Cancer Res.*, **23**, 7521–7530.
37. Konstantinopoulos,P.A., Ceccaldi,R., Shapiro,G.I. and D'Andrea,A.D. (2015) Homologous recombination deficiency: exploiting the fundamental vulnerability of ovarian cancer. *Cancer Discov.*, **5**, 1137–1154.
38. Takaya,H., Nakai,H., Takamatsu,S., Mandai,M. and Matsumura,N. (2020) Homologous recombination deficiency status-based classification of high-grade serous ovarian carcinoma. *Sci. Rep.*, **10**, 2757.
39. Pennington,K.P., Walsh,T., Harrell,M.I., Lee,M.K., Pennil,C.C., Rendi,M.H., Thornton,A., Norquist,B.M., Casadei,S., Nord,A.S., *et al.* (2014) Germline and somatic mutations in homologous recombination genes predict platinum response and survival in ovarian, fallopian tube, and peritoneal carcinomas. *Clin. Cancer Res.*, **20**, 764–775.
40. Lhotova,K., Stolarova,L., Zemankova,P., Vocka,M., Janatova,M., Borecka,M., Cerna,M., Jelinkova,S., Kral,J., Volkova,Z., *et al.* (2020) Multigene panel germline testing of 1333 Czech patients with ovarian cancer. *Cancers (Basel)*, **12**, 956.
41. Coleman,R.L., Oza,A.M., Lorusso,D., Aghajanian,C., Oaknin,A., Dean,A., Colombo,N., Weberpals,J.I., Clamp,A., Scambia,G., *et al.* (2017) Rucaparib maintenance treatment for recurrent ovarian carcinoma after response to platinum therapy (ARIEL3): a randomised, double-blind, placebo-controlled, phase 3 trial. *Lancet (London, England)*, **390**, 1949–1961.
42. Naipal,K.A.T., Verkaik,N.S., Ameziane,N., Van Deurzen,C.H.M., Brugge,P.T., Meijers,M., Sieuwerts,A.M., Martens,J.W., O'Connor,M.J., Vrieling,H., *et al.* (2014) Functional ex vivo assay to select homologous recombination-deficient breast tumors for PARP inhibitor treatment. *Clin. Cancer Res.*, **20**, 4816–4826.
43. Haaf,T., Golub,E.I., Reddy,G., Radding,C.M. and Ward,D.C. (1995) Nuclear foci of mammalian Rad51 recombination protein in somatic cells after DNA damage and its localization in synaptonemal complexes. *Proc. Natl Acad. Sci. U.S.A.*, **92**, 2298–2302.
44. Meijer,T.G., Verkaik,N.S., Sieuwerts,A.M., Van Riet,J., Naipal,K.A.T., Van Deurzen,C.H.M., Den Bakker,M.A., Sleddens,H.F.B.M., Dubbink,H.J., Dorine den Toom,T., *et al.* (2018) Functional *ex vivo* assay reveals homologous recombination deficiency in breast cancer beyond BRCA gene defects. *Clin. Cancer Res.*, **24**, 6277–6287.
45. Castroviejo-Bermejo,M., Cruz,C., Llop-Guevara,A., Gutiérrez-Enríquez,S., Ducy,M., Ibrahim,Y.H., Gris-Oliver,A., Pellegrino,B., Bruna,A., Guzmán,M., *et al.* (2018) A RAD51 assay feasible in routine tumor samples calls PARP inhibitor response beyond BRCA mutation. *EMBO Mol. Med.*, **10**, e9172.
46. Cruz,C., Castroviejo-Bermejo,M., Gutiérrez-Enríquez,S., Llop-Guevara,A., Ibrahim,Y.H., Gris-Oliver,A., Bonache,S., Morancho,B., Bruna,A., Rueda,O.M., *et al.* (2018) RAD51 foci as a functional biomarker of homologous recombination repair and PARP inhibitor resistance in germline BRCA-mutated breast cancer. *Ann. Oncol.*, **29**, 1203–1210.
47. Meijer,T.G., Verkaik,N.S., van Deurzen,C.H.M., Dubbink,H.-J., den Toom,T.D., Sleddens,H.F.B.M., De Hoop,E.O., Dinjens,W.N.M., Kanaar,R., van Gent,D.C., *et al.* (2019) Direct ex vivo observation of homologous recombination defect reversal after DNA-damaging chemotherapy in patients with metastatic breast cancer. *JCO Precis. Oncol.*, **3**, 1–12.
48. Tumiati,M., Hietanen,S., Hynninen,J., Pietila,E., Farkkil,A., Kaipio,K., Roering,P., Huhtinen,K., Alkodsi,A., Li,Y., *et al.* (2018) A functional homologous recombination assay predicts primary chemotherapy response and long-term survival in ovarian cancer patients. *Clin. Cancer Res.*, **24**, 4482–4493.
49. Mukhopadhyay,A., Elattar,A., Cerbinskaite,A., Wilkinson,S.J., Drew,Y., Kyle,S., Los,G., Hostomsky,Z., Edmondson,R.J. and Curtin,N.J. (2010) Development of a functional assay for homologous recombination status in primary cultures of epithelial ovarian tumor and correlation with sensitivity to poly(ADP-ribose) polymerase inhibitors. *Clin. Cancer Res.*, **16**, 2344–2351.
50. Alkema,N.G., Tomar,T., Duiker,E.W., Jan Meersma,G., Klip,H., van der Zee,A.G.J., Wisman,G.B.A. and de Jong,S. (2015) Biobanking of patient and patient-derived xenograft ovarian tumour tissue: efficient preservation with low and high fetal calf serum based methods. *Sci. Rep.*, **5**, 14495.
51. Fokkema,I.F.A.C., Kroon,M., López Hernández,J.A., Asscheman,D., Lugtenburg,I., Hoogenboom,J. and den Dunnen,J.T. (2021) The LOVD3 platform: efficient genome-wide sharing of genetic variants. *Eur. J. Hum. Genet.*, **29**, 1796–1803.
52. Schouten,P.C., Richters,L., Vis,D.J., Kommoss,S., Dijk,E.V., Ernst,C., Kluin,R.J.C., Marm,F.M., Lips,E.H., Schmidt,S., *et al.* (2021) Ovarian cancer-specific BRCA-like copy-number aberration classifiers detect mutations associated with homologous recombination deficiency in the AGO-TR1 trial. *Clin. Cancer Res.*, **27**, 6559–6569.
53. Ter Brugge,P., Kristel,P., van der Burg,E., Boon,U., de Maaker,M., Lips,E., Mulder,L., de Ruiter,J., Moutinho,C., Gevensleben,H., *et al.* (2016) Mechanisms of therapy resistance in patient-derived xenograft models of BRCA1-deficient breast cancer. *J. Natl. Cancer Inst.*, **108**, 1075.
54. Eisenhauer,E.A., Therasse,P., Bogaerts,J., Schwartz,L.H., Sargent,D., Ford,R., Dancey,J., Arbuck,S., Gwyther,S., Mooney,M., *et al.* (2008) New response evaluation criteria in solid tumours: revised RECIST guideline (version 1.1). *Eur. J. Cancer*, **45**, 228–247.
55. van Wijk,L.M., Vermeulen,S., Meijers,M., van Diest,M.F., Ter Haar,N.T., de Jonge,M.M., Solleveld-Westerink,N., van Wezel,T., van Gent,D.C., Kroep,J.R., *et al.* (2020) The RECAP test rapidly and reliably identifies homologous recombination-deficient ovarian carcinomas. *Cancers (Basel).*, **12**, 2805.
56. Fu,H. and Aladjem,M.I. (2022) DNA replication profiling by molecular combing on single DNA fibers. *STAR Protoc.*, **3**, 101290.
57. Soukupova,J., Zemankova,P., Lhotova,K., Janatova,M., Borecka,M., Stolarova,L., Lhota,F., Foretova,L., Machackova,E., Stranecky,V., *et al.* (2018) Validation of CZECANCA (CZEch CAncer paNel for Clinical Application) for targeted NGS-based analysis of hereditary cancer syndromes. *PLoS One*, **13**, e0195761.
58. Fugger,K., Bajrami,I., Silva Dos Santos,M., Young,S.J., Kunzelmann,S., Kelly,G., Hewitt,G., Patel,H., Goldstone,R., Carell,T., *et al.* (2021) Targeting the nucleotide salvage factor DNPH1 sensitizes BRCA-deficient cells to PARP inhibitors. *Science*, **372**, 156–165.
59. Kaufman,B., Shapira-Frommer,R., Schmutzler,R.K., Audeh,M.W., Friedlander,M., Balmaña,J., Mitchell,G., Fried,G., Stemmer,S.M., Hubert,A., *et al.* (2015) Olaparib monotherapy in patients with advanced cancer and a germline BRCA1/2 mutation. *J. Clin. Oncol.*, **33**, 244–250.
60. Vollebergh,M.A., Lips,E.H., Nederlof,P.M., Wessels,L.F.A., Wesseling,J., Vd Vijver,M.J., de Vries,E.G.E., van Tinteren,H., Jonkers,J., Hauptmann,M., *et al.* (2014) Genomic patterns resembling BRCA1- and BRCA2-mutated breast cancers predict benefit of intensified carboplatin-based chemotherapy. *Breast Cancer Res.*, **16**, R47.
61. Compadre,A.J., van Biljon,L.N., Valentine,M.C., Llop-Guevara,A., Graham,E., Fashemi,B., Herencia-Ropero,A., Kotnik,E.N., Cooper,I., Harrington,S.P., *et al.* (2023) RAD51 Foci as a biomarker predictive of platinum chemotherapy response in ovarian cancer. *Clin. Cancer Res.*, **29**, 2466–2479.
62. Torres-Esquius,S., Llop-Guevara,A., Gutiérrez-Enríquez,S., Romey,M., Teulé,À., Llort,G., Herrero,A., Sánchez-Henarejos,P., Vallmajó,A., González-Santiago,S., *et al.* (2024) Prevalence of homologous recombination deficiency among patients with germline RAD51C/D breast or ovarian cancer. *JAMA Netw. Open*, **7**, e247811.

63. Ström,C.E., Johansson,F., Uhlén,M., Szigyarto,C.A.-K., Erixon,K. and Helleday,T. (2011) Poly (ADP-ribose) polymerase (PARP) is not involved in base excision repair but PARP inhibition traps a single-strand intermediate. *Nucleic Acids Res.*, **39**, 3166–3175.
64. Zhong,A., Zhang,H., Xie,S., Deng,M., Zheng,H., Wang,Y., Chen,M., Lu,R. and Guo,L. (2018) Inhibition of MUS81 improves the chemical sensitivity of olaparib by regulating MCM2 in epithelial ovarian cancer. *Oncol. Rep.*, **39**, 1747–1756.
65. Zimmermann,M., Murina,O., Reijns,M.A.M., Agathanggelou,A., Challis,R., Tarnauskaite,Ž., Muir,M., Fluteau,A., Aregger,M., McEwan,A., *et al.* (2018) CRISPR screens identify genomic ribonucleotides as a source of PARP-trapping lesions. *Nature*, **559**, 285–289.
66. Mateo,J., Carreira,S., Sandhu,S., Miranda,S., Mossop,H., Perez-Lopez,R., Nava Rodrigues,D., Robinson,D., Omlin,A., Tunariu,N., *et al.* (2015) DNA-repair defects and olaparib in metastatic prostate cancer. *N. Engl. J. Med.*, **373**, 1697–1708.
67. Lheureux,S., Bruce,J.P., Burnier,J.V., Karakasis,K., Shaw,P.A., Clarke,B.A., Yang,S.Y.C., Quevedo,R., Li,T., Dowar,M., *et al.* (2017) Somatic BRCA1/2 recovery as a resistance mechanism after exceptional response to poly (ADP-ribose) polymerase inhibition. *J. Clin. Oncol.*, **35**, 1240–1249.
68. Feng,W. and Jasin,M. (2017) BRCA2 suppresses replication stress-induced mitotic and G1 abnormalities through homologous recombination. *Nat. Commun.*, **8**, 525.
69. Chen,M., van den Tempel,N., Bhattacharya,A., Yu,S., Rutgers,B., Fehrmann,R.S.N., de Haas,S., van der Vegt,B. and van Vugt,M.A. (2024) Functional ex vivo DNA fibre assay to measure replication dynamics in breast cancer tissue. *J. Pathol.*, **264**, 90–100.

Received: May 21, 2024. **Revised:** October 23, 2024. **Editorial Decision:** October 25, 2024. **Accepted:** October 28, 2024